

Supersymmetric Nonlinear $O(3)$ Sigma Model on the Lattice

Raphael Flore, Daniel Körner, Andreas Wipf, Christian Wozar

*Theoretisch-Physikalisches Institut, Universität Jena,
Fröbelstieg 1, D-07743 Jena, Germany*

E-mail: Raphael.Flore@uni-jena.de, Daniel.Koerner@uni-jena.de,
wipf@tpi.uni-jena.de, christian.wozar@vega.de

ABSTRACT: A supersymmetric extension of the nonlinear $O(3)$ sigma model in two spacetime dimensions is investigated by means of Monte Carlo simulations. We argue that it is impossible to construct a lattice action that implements both the $O(3)$ symmetry as well as at least one supersymmetry exactly at finite lattice spacing. It is shown by explicit calculations that previously proposed discretizations fail to reproduce the exact symmetries of the target manifold in the continuum limit. We provide an alternative lattice action with exact $O(3)$ symmetry and compare two approaches based on different derivative operators. Using the nonlocal SLAC derivative for the quenched model on moderately sized lattices we extract the value $\sigma(2, u_0) = 1.2604(13)$ for the step scaling function at $u_0 = 1.0595$, to be compared with the exact value 1.261210. For the supersymmetric model with SLAC derivative the discrete chiral symmetry is maintained but we encounter strong sign fluctuations, rendering large lattice simulations ineffective. By applying the Wilson prescription, supersymmetry and chiral symmetry are broken explicitly at finite lattice spacing, though there is clear evidence that both are restored in the continuum limit by fine tuning of a single mass parameter.

KEYWORDS: Extended Supersymmetry, Lattice Quantum Field Theory, Sigma Models, Field Theories in Lower Dimensions

Contents

1	Introduction	2
2	Symmetries and possible discretizations of the $O(N)$ nonlinear sigma model	3
2.1	Constrained and unconstrained formulations	3
2.2	Extended supersymmetry of the $O(3)$ -model	5
2.3	Discretization and constraints	5
2.3.1	Stereographic projection and measure of path integration	6
2.3.2	Coset formulation	6
2.3.3	Fermion determinant	7
2.4	Lattice derivatives	8
2.4.1	SLAC derivative	8
2.4.2	Wilson derivative	8
2.4.3	Universality and the SLAC derivative	8
2.5	Supersymmetries on the lattice	11
3	Numerical results	13
3.1	Drawbacks of a Q -exact lattice formulation	13
3.2	$O(3)$ symmetric formulations	17
3.3	Fermionic masses	18
3.4	Chiral symmetry breaking	19
3.5	Bosonic masses	20
3.6	Fine tuning of the Wilson derivative	22
3.7	Path integral based Ward identity	25
4	Conclusion	27
A	Conventions and Fierz identities	28
B	Invariance of the action under the second supersymmetry	28
C	Transformation of the discretized measure	29
D	Sign of the fermion determinant	30
E	Algorithmic aspects	31

1 Introduction

Despite its great success in the description of high energy experiments, the Standard Model of particle physics still faces serious problems, especially with regard to cosmological observations, where yet undiscovered sources of gravitation are proposed to correct the seemingly unbalanced equation of observed matter on the one hand and gravitational attraction on the other hand [1]. Another interesting question concerns the existence of far more matter than antimatter in our universe, and this fact is connected to the strong CP problem (see [2] and references listed therein). Coined as the hierarchy problem is the question of scales that are involved in the fundamental theory of particle physics. To address these open issues, extensions of the Standard Model have been proposed, among them supersymmetrically extended versions, in particular the Minimal Supersymmetric Standard Model (MSSM). It is of great interest to examine the nonperturbative properties of this theory, but the utilization of the only ab initio method for this purpose, namely a spacetime lattice simulation, is notoriously difficult because of the many different scales that are involved.

In the past, two-dimensional nonlinear sigma models have been applied successfully to model nonperturbative properties of four-dimensional strongly coupled pure gauge theories [3]. Similarly one may employ the supersymmetrized version of the nonlinear sigma model to effectively describe super-Yang-Mills theories with a strongly interacting fermionic sector. A first construction of the supersymmetric nonlinear sigma model with $O(N)$ target manifold is due to E. Witten [4] and P. Di Vecchia and S. Ferrara [5], followed by a number of papers that established analytical properties, including asymptotic safety, spontaneous breaking of chiral symmetry and the dynamical generation of particle masses [6–8]. Further studies are particularly concerned with the special case of the $O(3)$ model, which admits an extended $\mathcal{N}=2$ supersymmetry algebra since its target manifold is Kähler [9].

This enhanced supersymmetry has recently raised some interest with regard to the endeavor to study supersymmetric theories by numerical simulations. Because it is an extension of the Poincaré symmetry, any lattice discretization of spacetime also breaks supersymmetry. This can be traced back to the failure of the Leibniz rule on the lattice [10]. It is therefore necessary to take great care in restoring the full symmetry in the continuum limit. In general, one needs to introduce appropriate counter terms for each relevant supersymmetry-breaking operator that must each be fine tuned such that the desired continuum theory is reached [11]. Depending on the number of parameters, this becomes practically impossible very fast due to limited computer time. In addition, much information about the theory is needed prior to numerical investigations. For that reason alternative approaches have been proposed in order to reduce the number of fine tuning parameters or even render the fine tuning procedure obsolete [12]. One such approach for theories with extended supersymmetry aims at the construction of a nilpotent charge composed from the supercharges such that both the continuum as well as the discretized model are invariant under this charge. It is then expected that, by preserving a part of the symmetry, invariance under the full supersymmetry is restored automatically in the continuum limit, without the need for fine tuning. This procedure was applied to the supersymmetric $O(3)$ model [13, 14] and the authors conclude that the supersymmetric Ward identities are indeed fulfilled in the continuum limit, hinting at a restoration of the full supersymmetry. However, the lattice discretization constructed in this way breaks the $O(3)$ symmetry of the target space explicitly at finite lattice spacing and no attempt was made to show that it is restored in the

continuum limit. It is therefore unclear whether this discretization actually describes the correct model in the continuum and we will address this question in much detail.

Expensive dynamical fermion simulations are needed in order to treat the superpartners on equal footing and we wish to utilize the SLAC prescription for the fermionic derivative, which performed very well in previously examined Wess-Zumino models [15], showing greatly reduced lattice artifacts in comparison to e.g. the Wilson derivative. Furthermore, the SLAC derivative allows for a discretized action that does not break the discrete chiral symmetry explicitly. But this comes at the cost of having a nonlocal derivative operator and we will explicitly check whether the SLAC derivative is applicable in the present model. In order to compare with an alternative, the model will also be studied by simulations based on the Wilson derivative, which is less affected by the sign problem and enables us to investigate larger lattices.

The article is organized as follows: We introduce the supersymmetric version of the nonlinear $O(3)$ model along with a derivation of its stereographic projection in the superfield formalism. We then discuss the extended supersymmetry of the model and express the related transformations in terms of constrained fields. Based on the continuum theory two alternative discretizations in Euclidean space are presented which resolve the field constraints – one using stereographically projected fields and the other using elements of the orthogonal group $SO(3)$. Thus providing the basic setup of our lattice discretization, we go on to argue that the SLAC derivative is indeed applicable here by performing a high precision analysis of the step scaling function in the quenched model. Towards the end of the first part we finally answer the question whether a lattice theory exists that admits both the $O(3)$ symmetry and at least one supersymmetry.

In the second part, which is primarily dedicated to extensive numerical investigations, we discuss the missing target space symmetry in a previously given lattice discretization by Catterall et al. [13] and proceed with results from our own calculations. We examine the discrete chiral symmetry as well as supersymmetry by presenting results for the chiral condensate and the masses of the elementary excitations computed from ensembles obtained with both SLAC and Wilson derivative. In the second case special emphasis is put on the fine tuning of divergent operators in order to arrive at a supersymmetric continuum limit. Before coming to our conclusions, we present our results for a simple Ward identity based on the expectation value of the bosonic action.

2 Symmetries and possible discretizations of the $O(N)$ nonlinear sigma model

2.1 Constrained and unconstrained formulations

The supersymmetric extension of the nonlinear $O(N)$ sigma model in two-dimensional Euclidean spacetime can be formulated in terms of a real superfield ¹,

$$\Phi = n + i\bar{\theta}\psi + \frac{i}{2}\bar{\theta}\theta f, \quad (2.1)$$

subject to the constraint $\Phi\Phi = 1$, where n and f are N -tuples of real scalar fields and ψ is an N -tuple of Majorana fields. We shall refer to the elements of a tuple as “flavors”. The constraint in superspace is equivalent to the following constraints for the component fields,

$$n^2 = 1, \quad n\psi = 0 \quad \text{and} \quad nf = \frac{i}{2}\bar{\psi}\psi. \quad (2.2)$$

¹Conventions concerning the Gamma matrices and the Fierz relations are explained in appendix A.

The $O(N)$ -invariant Lagrangian density is defined in terms of the covariant derivatives $D_\alpha = \partial_{\bar{\theta}\alpha} + i(\gamma^\mu \theta)_\alpha \partial_\mu$,

$$\mathcal{L} = \frac{1}{2g^2} \overline{D\Phi} D\Phi|_{\bar{\theta}\theta} = \frac{1}{2g^2} (\partial_\mu \mathbf{n} \partial^\mu \mathbf{n} + i\bar{\psi} \not{\partial} \psi - \mathbf{f}^2) . \quad (2.3)$$

The equation of motion for the auxiliary field implies that \mathbf{f} and \mathbf{n} are parallel, $\mathbf{f} = \frac{i}{2}(\bar{\psi}\psi)\mathbf{n}$, and the resulting on-shell Lagrangian density contains a 4-Fermi term,

$$\mathcal{L} = \frac{1}{2g^2} (\partial_\mu \mathbf{n} \partial^\mu \mathbf{n} + i\bar{\psi} \not{\partial} \psi + \frac{1}{4}(\bar{\psi}\psi)^2) . \quad (2.4)$$

The action and the constraints are both invariant under global $O(N)$ “flavor” transformations and by construction they are also invariant under the $\mathcal{N} = 1$ supersymmetry transformations

$$\delta \mathbf{n} = i\bar{\varepsilon} \psi, \quad \delta \psi = (\not{\partial} + \frac{i}{2}\bar{\psi}\psi) \mathbf{n} \varepsilon . \quad (2.5)$$

Besides flavor symmetry and supersymmetry the classical theory admits a further \mathbb{Z}_2 -symmetry generated by the chiral transformation $\psi \rightarrow i\gamma_* \psi$. However, quantum fluctuations dynamically generate a mass term and hence induce spontaneous breaking of the chiral \mathbb{Z}_2 -symmetry.

Explicit constraints for the fields are sometimes difficult to handle, e.g. in numerical simulations. Therefore, it is useful to construct a formulation of the model in terms of an unconstrained real superfield $U(x, \theta) = \mathbf{u}(x) + i\bar{\theta}\boldsymbol{\lambda}(x) + \frac{i}{2}\bar{\theta}\theta \mathbf{g}(x)$, which is an $(N-1)$ -tupel. It is related to the superfield Φ by a stereographic projection in superspace

$$\begin{pmatrix} \Phi_1 \\ \Phi_\perp \end{pmatrix} = \frac{1}{1+U^2} \begin{pmatrix} 1-U^2 \\ 2U \end{pmatrix} . \quad (2.6)$$

The decomposition of the projection into bosonic and fermionic fields reads:

$$\mathbf{n}_\perp = 2\rho \mathbf{u}, \quad \psi_\perp = 2\rho \boldsymbol{\lambda} - 4\rho^2 (\mathbf{u}\boldsymbol{\lambda}) \mathbf{u} \quad \text{with} \quad \rho = \frac{1}{1+\mathbf{u}^2} . \quad (2.7)$$

The expressions for the remaining components n_1 and ψ_1 can be determined either from (2.6) or from (2.7) and the constraints $\mathbf{n}^2 = 1$ and $\mathbf{n}\psi = 0$. The inverse transformation in superspace reads $U = \Phi_\perp / (1 + \Phi_1)$ and leads to

$$\mathbf{u} = \frac{1}{2\rho} \mathbf{n}_\perp, \quad \boldsymbol{\lambda} = \frac{1}{2\rho} \psi_\perp - \frac{1}{4\rho^2} \psi_1 \mathbf{n}_\perp \quad \text{with} \quad \rho = \frac{1+n_1}{2} . \quad (2.8)$$

Applying the stereographic projection (2.7), the on-shell Lagrangian density can be written in terms of the unconstrained fields as

$$\mathcal{L} = \frac{2}{g^2} \rho^2 (\partial_\mu \mathbf{u} \partial^\mu \mathbf{u} + i\bar{\boldsymbol{\lambda}} \not{\partial} \boldsymbol{\lambda} + 4i\rho (\bar{\boldsymbol{\lambda}} \mathbf{u}) \gamma^\mu (\partial_\mu \mathbf{u} \boldsymbol{\lambda}) + \rho^2 (\bar{\boldsymbol{\lambda}} \boldsymbol{\lambda})^2) . \quad (2.9)$$

The action is invariant under the supersymmetry transformations

$$\delta \mathbf{u} = i\bar{\varepsilon} \boldsymbol{\lambda}, \quad \delta \boldsymbol{\lambda} = (\not{\partial} + i\rho \bar{\boldsymbol{\lambda}} \boldsymbol{\lambda}) \mathbf{u} \varepsilon - 2i\rho (\bar{\boldsymbol{\lambda}} \mathbf{u}) \boldsymbol{\lambda} \varepsilon . \quad (2.10)$$

2.2 Extended supersymmetry of the $O(3)$ -model

The fields \mathbf{u} and $\boldsymbol{\lambda}$ are unconstrained, but their target manifold has a non-trivial metric. In fact, for $N = 3$ the target manifold is Kähler and the corresponding potential can be written in terms of the complex field $u = u_1 + iu_2$ as $K(u, \bar{u}) = \ln(1 + \bar{u}u)$. As pointed out by Zumino a nonlinear sigma model whose target manifold is Kähler, possesses an $\mathcal{N}=2$ -supersymmetric extension [9]. Hence the $O(3)$ admits an additional supersymmetry besides (2.10) and (2.5).

In order to derive an explicit expression of this symmetry, we investigate a general ansatz in terms of the unconstrained fields ($\delta\mathbf{u} = i\bar{\varepsilon}(A_I)\boldsymbol{\lambda}$, etc.), and determine the constraints for the matrices A_I , etc., which follow from the supersymmetry algebra and the invariance of the action². This approach yields the second pair of symmetry transformations as

$$\begin{aligned}\delta\mathbf{u} &= \sigma_2 \bar{\varepsilon} \boldsymbol{\lambda} \\ \delta\boldsymbol{\lambda} &= i\sigma_2 (\not{\partial}\mathbf{u} - i\rho(\bar{\boldsymbol{\lambda}}\boldsymbol{\lambda})\mathbf{u} + 2i\rho(\bar{\boldsymbol{\lambda}}\mathbf{u})\boldsymbol{\lambda}) \varepsilon.\end{aligned}\tag{2.11}$$

Both supersymmetries (2.10, 2.11) can also be obtained by deriving the complex supersymmetry from the Kähler potential, cf. [9], and decomposing the complex fields and complex transformation parameters into real ones.

Applying (2.7) and (2.8), we can also express these transformations in terms of the constrained fields in order to determine the second supersymmetry of (2.4). One finds the simple transformations

$$\begin{aligned}\delta\mathbf{n} &= i\mathbf{n} \times \bar{\varepsilon}\boldsymbol{\psi} \\ \delta\boldsymbol{\psi} &= -\mathbf{n} \times \partial_\mu \mathbf{n} \gamma^\mu \varepsilon - i\bar{\varepsilon}\boldsymbol{\psi} \times \boldsymbol{\psi},\end{aligned}\tag{2.12}$$

where $\mathbf{a} \times \mathbf{b}$ denotes the vector product of \mathbf{a} and \mathbf{b} . A proof that the action (2.4) is invariant under these transformations is given in appendix B. The two on-shell supersymmetries (2.5, 2.12) are generated by the supercharges

$$\mathcal{Q}_I = i \int \gamma^\mu \gamma^0 \partial_\mu \mathbf{n} \boldsymbol{\psi} \quad , \quad \mathcal{Q}_{II} = -i \int \gamma^\mu \gamma^0 (\mathbf{n} \times \partial_\mu \mathbf{n}) \boldsymbol{\psi}.\tag{2.13}$$

These results are in agreement with the supercurrents constructed in [4].

2.3 Discretization and constraints

So far, sigma models in the continuum have been considered. In order to investigate the corresponding lattice models one should try to discretize it in a way that maintains as many symmetries of the continuum theory as possible. This is difficult with respect to supersymmetry, as will be discussed in section 2.5. But also the flavor symmetry must be treated with care: If one starts with an unconstrained formulation of the model and tries to discretize it in a straightforward way, one generically breaks the $O(N)$ symmetry. For the $O(3)$ model we will illustrate this in more detail in section 3.1. Simulations demonstrate clearly that even in the continuum limit the symmetry is

²An example of this approach can be found in [16], where it is applied to the Wess-Zumino model.

not restored in such cases. In order to avoid this problem, we start with a formulation in terms of constrained fields, whose discretization is manifestly $O(N)$ -invariant:

$$S[\mathbf{n}, \psi] = \frac{1}{2g^2} \sum_{x,y \in \Lambda} \left(\mathbf{n}_x^\top K_{xy} \mathbf{n}_y + i \bar{\psi}_x^\alpha M_{xy}^{\alpha\beta} \psi_y^\beta + \frac{1}{4} (\bar{\psi}_x \delta_{xy} \psi_y)^2 \right). \quad (2.14)$$

The subscripts x, y denote lattice sites, while α, β are spinor indices. The lattice derivatives K_{xy} and $M_{xy}^{\alpha\beta}$ are proportional to the identity in flavor space. The constraints $\mathbf{n}_x \mathbf{n}_x = 1$ and $\mathbf{n}_x \psi_x = 0$ must be fulfilled at each lattice point x and they are implemented as delta-functions in the path integral measure. This causes some difficulties in numerical simulations. One can cope with this problem by either applying the stereographic projection or by introducing group valued dynamical variables.

2.3.1 Stereographic projection and measure of path integration

The stereographic projection (2.7) resolves both constraints and leads to an unconstrained but yet $O(N)$ -symmetric lattice formulation:

$$\begin{aligned} S[\mathbf{u}, \boldsymbol{\lambda}] &= S_B + S_{2F} + S_{4F}, \text{ with} \\ S_B &= \frac{1}{2g^2} \sum_{x,y} 4\rho_x \mathbf{u}_x^T K_{xy} \mathbf{u}_y \rho_y + \rho_x (1 - \mathbf{u}_x^2) K_{xy} (1 - \mathbf{u}_y^2) \rho_y, \\ S_{2F} &= \frac{2i}{g^2} \sum_{x,y;\alpha,\beta} \bar{\lambda}_x^\alpha \left[(\rho - 2\rho^2 \mathbf{u} \mathbf{u}^T)_x M_{xy}^{\alpha\beta} (\rho - 2\rho^2 \mathbf{u} \mathbf{u}^T)_y + 4 (\rho^2 \mathbf{u})_x M_{xy}^{\alpha\beta} (\rho^2 \mathbf{u}^T)_y \right] \lambda_y^\beta, \\ S_{4F} &= \frac{2}{g^2} \sum_x \rho_x^4 (\bar{\lambda}_x \boldsymbol{\lambda}_x)^2. \end{aligned} \quad (2.15)$$

The change from the constrained fields (\mathbf{n}, ψ) to the unconstrained fields $(\mathbf{u}, \boldsymbol{\lambda})$ yields a non-trivial Jacobian which is computed in appendix C. The result is³:

$$\prod_{x \in \Lambda} d\mathbf{n}_x d\psi_x^1 d\psi_x^2 \delta(\mathbf{n}_x^2 - 1) \delta(\mathbf{n} \psi_x^1) \delta(\mathbf{n} \psi_x^2) \longrightarrow \prod_{x \in \Lambda} d\mathbf{u}_x d\lambda_x^1 d\lambda_x^2 (1 + \mathbf{u}_x^2)^{N-1}. \quad (2.16)$$

The four-fermion interaction can be eliminated by employing the usual Hubbard-Stratonovich transformation [17], which introduces an auxiliary bosonic field σ :

$$S[\mathbf{u}, \boldsymbol{\lambda}] = S_B + S_{2F} + \frac{1}{2g^2} \sum_{x \in \Lambda} (\sigma_x^2 + 4i\sigma_x \rho_x^2 \bar{\lambda}_x \boldsymbol{\lambda}_x) \quad (2.17)$$

2.3.2 Coset formulation

The constrained field \mathbf{n} propagates on the unit sphere $S^{N'}$ with $N' = N - 1$ which can be viewed as coset space $SO(N)/SO(N')$. To relate the constrained field to an element of the orthogonal group $SO(N)$ we supplement at each lattice site the unit vector \mathbf{n} by orthonormal vectors $\mathbf{e}_1, \dots, \mathbf{e}_{N'}$

³One obtains the same result if one does not eliminate the auxiliary field f at the beginning but projects it in accordance to (2.6) and integrates out the unconstrained auxiliary field g afterwards. Following this approach, the superdeterminant yields only a trivial factor, while the density $1/\rho^{N-1}$ stems from integrating w.r.t. g .

such that $\{\mathbf{n}, \mathbf{e}_1, \dots, \mathbf{e}_{N'}\}$ forms an oriented orthonormal basis of \mathbb{R}^N . The N -component Majorana spinor orthogonal to \mathbf{n} is a linear combination of the \mathbf{e}_i , i.e.

$$\psi = \chi_1 \mathbf{e}_1 + \dots + \chi_{N'} \mathbf{e}_{N'}. \quad (2.18)$$

These N basis vectors may be viewed as columns of a rotation matrix $R = (\mathbf{n}, \mathbf{e}_1, \dots, \mathbf{e}_{N'})$ in N dimensions. Therefore the x -dependent orthonormal basis is given by a spacetime-dependent rotation $R \in \text{SO}(N)$ acting on a constant (x -independent) orthonormal frame $\{\mathbf{n}_0, \mathbf{g}_1, \dots, \mathbf{g}_{N'}\}$:

$$\mathbf{n}(x) = R(x)\mathbf{n}_0, \quad \mathbf{e}_i(x) = R(x)\mathbf{g}_i, \quad (2.19)$$

and the path integral in terms of new variables R , χ and σ reads

$$\mathcal{Z} = \int \mathcal{D}R \mathcal{D}\sigma \mathcal{D}\chi e^{-S_B - S_F} \quad (2.20)$$

with actions

$$S_B = \frac{1}{2g^2} \sum_{x,y} (\mathbf{n}_0^\top R_x^\top K_{xy} R_y \mathbf{n}_0 + \sigma_x \delta_{xy} \sigma_y), \quad S_F = \frac{i}{2g^2} \sum_{x,y} \chi_x^\top Q_{xy} \chi_y. \quad (2.21)$$

The action for the fermions contains the real and antisymmetric matrix

$$Q_{xy,ij} = \mathbf{g}_i^\top R_x^\top C M_{xy} R_y \mathbf{g}_j + \delta_{xy} \delta_{ij} C \sigma_x. \quad (2.22)$$

The base vectors $\{\mathbf{g}_i\}$ (or $\{\mathbf{e}_i\}$) are not unique since any rotation in the plane orthogonal to \mathbf{n}_0 transforms an admissible set of base vectors into another admissible set. More precisely,

$$R \longrightarrow R' = RS, \quad \chi_i \longrightarrow \chi'_i = \chi_k S_{ki}, \quad \text{with} \quad S\mathbf{n}_0 = \mathbf{n}_0, \quad S_{ij} = \mathbf{g}_i^\top S \mathbf{g}_j$$

are local $\text{SO}(N')$ symmetries of the action (2.21). The measure of the path integral is not affected by the change of the dynamical fields from \mathbf{n} to R , i.e. a distribution of R according to the Haar measure on $\text{SO}(N)$ will lead to a uniform distribution of $\mathbf{n} = R\mathbf{n}_0$ on the sphere. This renders the structure of the lattice action rather simple. The price we pay is a local $\text{SO}(N')$ symmetry in the choice of the basis vectors \mathbf{e}_i .

2.3.3 Fermion determinant

The treatment of the fermion operator is very similar for stereographically projected or group valued variables and we will only depict the second case here. Performing the Grassmannian integral in (2.20) leads to the bosonic path integral

$$\mathcal{Z} = \int \mathcal{D}R \mathcal{D}\sigma \text{sign Pf}(Q) e^{-S_B + \ln|\text{Pf}(Q)|}, \quad (2.23)$$

and simulations are performed in the sign quenched ensemble. This means that the configurations are sampled according to the probability distribution defined by the exponential function. The sign of the Pfaffian is handled by reweighting. In this formulation the invariance of the path integral under the local $\text{SO}(N')$ transformation is obvious: The bosonic action and Haar measure are both invariant under the change of variables $R \rightarrow RS$ with $S\mathbf{n}_0 = \mathbf{n}_0$. The operator Q_{xy} transforms as $S_x^\top Q_{xy} S_y$, which leaves the Pfaffian invariant since $S = \otimes_x S_x$ cancels in the general relation $\text{Pf}(S^\top Q S) = \det(S) \text{Pf}(Q)$. In the simulations the effective fermionic action is rewritten according to $\ln|\text{Pf}(Q)| = \frac{1}{2} \ln \det(Q)$ and the hybrid Monte Carlo algorithm is used, such that the Hamiltonian evolution of the group valued R field is similar to the quenched case.

2.4 Lattice derivatives

Now we specify the lattice derivative for the fermions $M_{xy}^{\alpha\beta}$ and bosons K_{xy} in the $O(N)$ invariant formulation. We will use two different implementations, the SLAC derivative and the Wilson derivative, so that we can compare results.

2.4.1 SLAC derivative

With the help of discrete Fourier transformation on a finite $N_t \times N_s$ lattice Λ with N lattice sites one may motivate the SLAC derivative [18],

$$\frac{1}{\sqrt{N}} \sum_{p \in \Lambda^*} i p_\mu e^{i p x} \tilde{f}(p) = \sum_{y \in \Lambda} f(y) \left(\frac{1}{N} \sum_{p \in \Lambda^*} i p_\mu e^{i p(x-y)} \right) \equiv \sum_{y \in \Lambda} (\partial_\mu^{\text{SLAC}})_{xy} f(y), \quad (2.24)$$

where p is from the dual Lattice Λ^* . This non-local derivative has been proven to be useful in the context of Wess-Zumino models [15] and supersymmetric quantum mechanics [19, 20]. Because the formulations based on the SLAC derivative show only small lattice artifacts and do *not break* the \mathbb{Z}_2 chiral symmetry explicitly, we use this derivative for the supersymmetric nonlinear sigma model:

$$K_{xy} = - \sum_{\mu} (\partial_\mu^{\text{SLAC}})^2_{xy}, \quad M_{xy} = (\gamma^\mu \partial_\mu^{\text{SLAC}})_{xy}. \quad (2.25)$$

The SLAC-derivative leads to lattice models without doublers.

2.4.2 Wilson derivative

Another suitable choice that avoids fermion doublers is the Wilson derivative which introduces an additional momentum-dependent mass term that vanishes in the naive continuum limit,

$$M_{xy}^{\alpha\beta} = \gamma_\mu^{\alpha\beta} (\partial_\mu^{\text{sym}})_{xy} + \delta^{\alpha\beta} \frac{r a}{2} \Delta_{xy}, \quad (2.26)$$

where $\partial_\mu^{\text{sym}}$ is the symmetric lattice derivative, a the lattice spacing and Δ_{xy} the lattice Laplacian. We choose the bosonic derivative in a particular form that has demonstrated superior results in Wess-Zumino models [15],

$$K_{xy} = - \sum_{\mu} (\partial_\mu^{\text{sym}})^2_{xy} + \left(\frac{r a}{2} \Delta_{xy} \right)^2. \quad (2.27)$$

The Wilson prescription breaks chiral symmetry explicitly, but is ultralocal in contrast to the SLAC derivative.

2.4.3 Universality and the SLAC derivative

It is not obvious that the SLAC derivative can be used for models with curved target space. To justify its use we will first study the purely bosonic $O(3)$ -model with this derivative and test if the known continuum result with scaling of the finite volume mass gap m can be reproduced. A quantity accessible at finite volumes is the step scaling function introduced by Lüscher, Weisz and Wolff [21]. At finite spatial volume $L = a N_s$, the renormalization group invariant variable $m(N_s)L$

can be computed at large temporal extent. On every finite lattice the step scaling function Σ is then determined according to

$$\Sigma(2, u, N_s^{-1}) = m(2N_s)2L|_{m(N_s)L=u}, \quad (2.28)$$

where the condition $m(N_s)L = u$ determines the bare coupling g^{-2} that is used on both spatial volumes N_s and $2N_s$.

One has to measure the finite volume mass gap m twice in order to determine Σ at a given N_s . First one has to tune the bare coupling until mL is u on the small lattice with N_s spatial sites. Then one goes to the larger lattice with $2N_s$ sites and measures $m(2N_s)2L_s$ with the previously determined bare coupling. The lattice step scaling function is expected to have a universal continuum limit

$$\sigma(2, u) = \Sigma(2, u, 0) = \lim_{N_s \rightarrow \infty} \Sigma(2, u, N_s^{-1})$$

and the high-precision results in [22, 23] demonstrate this universal behaviour. Here, the step scaling function is computed using the SLAC derivative. Following [21] we use $u_0 = 1.0595$ which, according to [24], leads to the continuum value

$$\sigma(2, u_0) = 1.261210. \quad (2.29)$$

Using the SLAC derivative the regularized action is given by

$$S = -\frac{1}{2g^2} \sum_{x,y} \mathbf{n}_0^T R_x^T (\partial_\mu^{\text{SLAC}})^2_{xy} R_y \mathbf{n}_0, \quad (2.30)$$

where R is the group valued dynamical field. Since the action is not given by nearest neighbour interactions, a cluster algorithm is not applicable and the hybrid Monte-Carlo algorithm will be used instead. The momenta of the ‘Hamiltonian’ used for the hybrid Monte-Carlo algorithm are elements of the Lie algebra $so(3)$.

The $O(3)$ invariant correlator is naturally defined as

$$C(t) = N_s^{-2} \sum_{x,y} \langle \mathbf{n}_{(t,x)} \mathbf{n}_{(0,y)} \rangle \quad (2.31)$$

and the mass is extracted via a fit to

$$C(t) \propto \cosh(ma(t - N_t/2)) \quad (2.32)$$

on a logarithmic scale, so that contributions from t ’s near $N_t/2$ are taken into account, where the contributions of the higher excited states are suppressed. However, reliable high-precision results can only be obtained if systematic errors are under control. To actually see the contribution of higher excited states, one considers the extracted mass as a function of t_0 where the fit is performed

N_s	$\Sigma(2, u_0, N_s^{-1})$	g^{-2}
4	1.28914(19)	1.22906(6)
6	1.27938(18)	1.31071(5)
8	1.27368(34)	1.36526(9)
10	1.27049(31)	1.40622(8)
12	1.26742(33)	1.43903(8)
16	1.26587(35)	1.48986(8)
20	1.26416(70)	1.52870(12)

Table 1. Value of the step scaling function $\Sigma(2, u_0, N_s^{-1})$ after interpolating to $u_0 = 1.0595$ for different spatial lattice sizes N_s and corresponding g^{-2} at which $m(N_s)L = u_0$ is reached.

over a range $t \in [t_0, N_t - t_0]$ for fixed N_t and N_s . This effect is analysed for $N_s \in \{6, 12\}$ and $N_t = 6N_s$ for a coupling $g^{-2} = 1.309$, which is quite close to the point of interest (2.29), with extremely large statistics of about $5 \cdot 10^9$ configurations, distributed over 1 000 replica. The results depicted in Fig. 1 show that for larger lattices the contribution of higher excited states is well below the usual statistical accuracy that is used for most of the results given below. For small lattices there are two competing effects: For *small* t_0 the contribution of higher states is well visible, whereas for *large* t_0 the well-known fluctuations arising from the non-locality of the SLAC derivative begin to grow. Therefore the optimal choice leading to systematic errors of the same order as the statistical ones, is given by $t_0 = N_s$ and will be used in the following. The second possible systematic error is due to the finite N_t . For N_t too small a thermal contribution to the mass gap will show up. This effect is investigated by keeping $t_0 = N_s$ fixed but varying N_t , see Fig. 2 for $N_s \in \{6, 12\}$. For the smaller lattice the contributions at small N_t are more pronounced and become negligible for $N_t > 6N_s$ while for the larger lattice $N_t > 5N_s$ is sufficient. To suppress these systematic errors $N_t = 8N_s$ ($N_t = 6N_s$) is used on the smaller (larger) lattice of each step scaling computation.

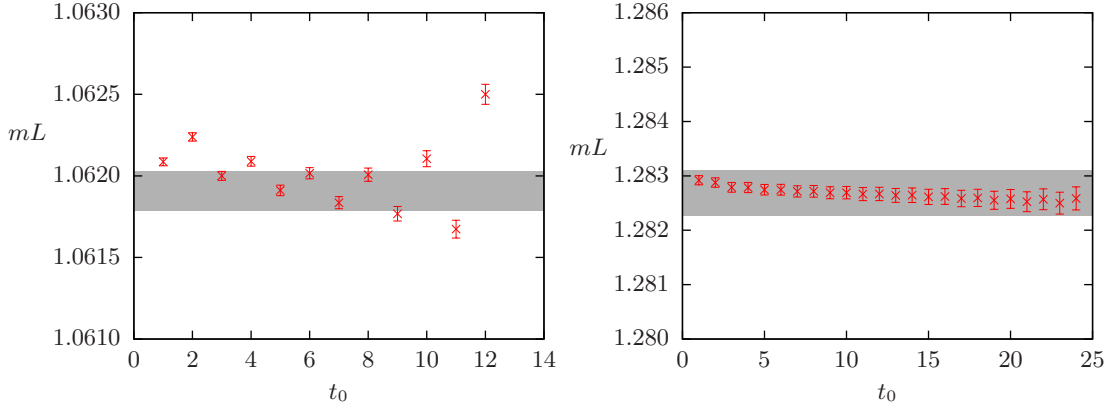


Figure 1. Mass gap extracted from a logarithmic cosh fit of the correlator (2.31) in a range $t \in [t_0, N_t - t_0]$ for $N_s = 6$ (left panel) and $N_s = 12$ (right panel) at coupling $g^{-2} = 1.309$ for fixed $N_t = 6N_s$. The shaded area denotes the usual accuracy of results at other g^{-2} .

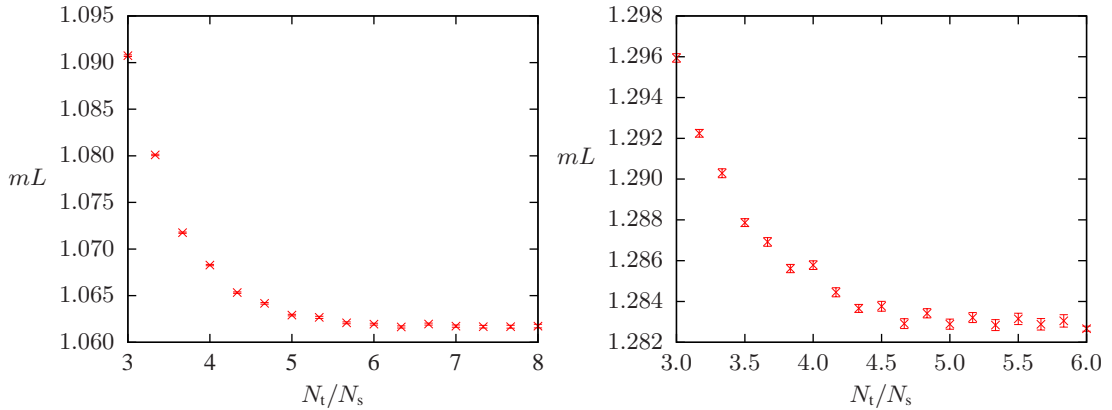


Figure 2. Mass gap extracted from a logarithmic cosh fit of the correlator (2.31) in a range $t \in [N_s, N_t - N_s]$ for $N_s = 6$ (left panel) and $N_s = 12$ (right panel) at coupling $\beta = 1.309$ for different N_t/N_s .

With the systematic errors under control it is possible to extrapolate the lattice step scaling function to the continuum limit. The bare coupling is tuned such that $u = m(N_s)L$ is near $u_0 = 1.0595$ on lattices with sizes $N_s \in \{4, 6, 8, 10, 12, 16, 20\}$. The corresponding $\Sigma(2, u, N_s^{-1})$ are plotted over u for a subset of these N_s in Fig. 3 (left panel), and a linear interpolation based on seven different coupling g^{-2} allows for the extraction of $\Sigma(2, u_0, N_s^{-1})$ at the point $u_0 = 1.0595$. The explicit values are collected in Tab. 1. With Symanzik’s theory of lattice artefacts it has been argued in [22] that finite a corrections are of order $\mathcal{O}(a^2(\ln a)^3)$ and appear *nearly linear* for a large range of computationally accessible lattice sizes [25]. For that reason an extrapolation to $a = 0$ based on the formula

$$\Sigma(2, u_0, N_s^{-1}) = \sigma(2, u_0) + A \left(\frac{B}{N_s} \right)^2 \left(\ln \frac{B}{N_s} \right)^3 \quad (2.33)$$

is used. The results for $N_t = 4$ have been omitted because of the large systematic errors introduced by the fluctuations arising from the SLAC derivative for large lattice spacings. The extrapolation is shown in Fig. 3 (right panel) and a value of $\sigma(2, u_0) = 1.2604(13)$ is extracted. This value is in complete agreement with the exactly known result in the continuum limit, see eq. (2.29). Therefore a discretisation of the (bosonic) $O(3)$ nonlinear sigma model with the SLAC derivative is feasible and may also be used for the supersymmetric model.

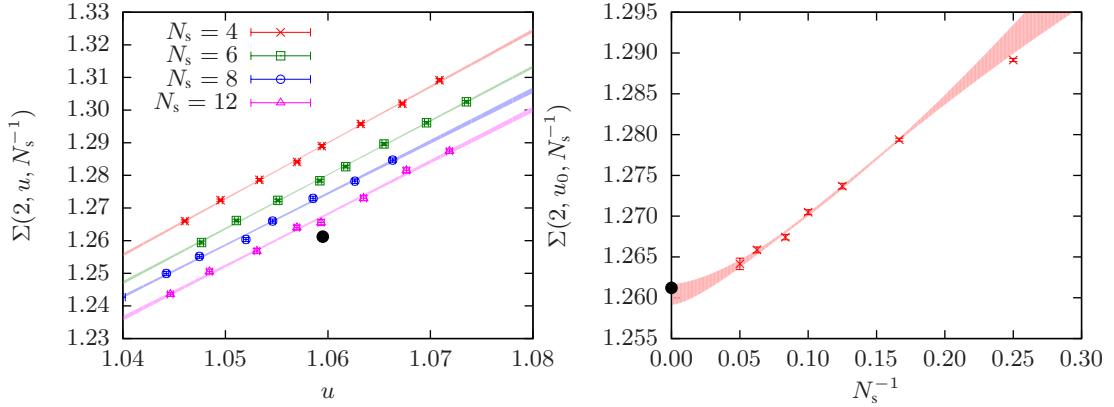


Figure 3. Left panel: Step scaling function for lattices with spatial size $N_s \in \{4, 6, 8, 12\}$. Shaded regions indicate error bounds of a linear interpolation. Right panel: Continuum limit of the step scaling function for $u_0 = 1.0595$. The shaded area indicates the error bounds of a fit according to Eq. (2.33), where the value for $N_s^{-1} = 0.25$ has been omitted. The black dot marks the continuum value given in Eq. (2.29).

2.5 Supersymmetries on the lattice

Is it possible to discretize the supersymmetric nonlinear $O(3)$ -model such that its characteristic symmetries are maintained? We have seen that it is straightforward to find a manifestly $O(3)$ -symmetric discretization. The treatment of supersymmetry on the lattice is more difficult, because it is an extension of the Poincaré symmetry, which is broken by any discretization of spacetime. However, there are some approaches to maintain at least a part of the supersymmetry on the lattice. One of these approaches relies on a twisting of the supersymmetry in a way that provides a *nilpotent* supercharge \mathcal{Q} which is used to find a \mathcal{Q} -exact formulation $S = \mathcal{Q}\Lambda$ of the lattice action. By construction this action is invariant under supersymmetries generated by \mathcal{Q} . This approach has

been applied to the $O(3)$ -NLSM in [13, 14]. However, the authors employ a formulation of the model in terms of unconstrained fields and its discretization breaks the $O(3)$ symmetry in such a way that it is not restored in the continuum limit. We will demonstrate this explicitly in section 3.1. We must thus conclude that the continuum limits of these lattice constructions cannot be identified with the two-dimensional non-linear $O(3)$ sigma model.

Are there other ways to find a partly supersymmetric but still $O(3)$ symmetric discretization? A symmetry of the model has to be a symmetry of the action (2.3), but is also has to be compatible with the constraints $\mathbf{n}^2 = 1$ and $\mathbf{n}\psi = 0$. Any supersymmetry has to be a combination of the transformations given in (2.5) and (2.12). If we consider the discretization of these, we notice that the first transformation (2.5) breaks the constraint $\mathbf{n}\psi = 0$ on the lattice, because

$$\delta_I(\mathbf{n}_x \psi_x^\alpha) = i\bar{\varepsilon} \psi_x \psi_x^\alpha + \sum_{y \in \Lambda} \mathbf{n}_x D_{xy}^{\alpha\beta} \mathbf{n}_y \varepsilon^\beta + \frac{i}{2} (\bar{\psi}_x \psi_x) \mathbf{n}_x^2 \varepsilon^\alpha \stackrel{(A.4)}{=} \sum_{y \in \Lambda} \mathbf{n}_x D_{xy}^{\alpha\beta} \mathbf{n}_y \varepsilon^\beta \quad (2.34)$$

does not vanish for arbitrary \mathbf{n}_x , no matter which derivative D_{xy} we use⁴. In contrast, the second transformation respects the constraints at each point:

$$\begin{aligned} \delta_{II}(\mathbf{n}_x \psi_x^\alpha) &= i(\mathbf{n}_x \times \bar{\varepsilon} \psi_x) \psi_x^\alpha - \sum_{y \in \Lambda} \mathbf{n}_x (\mathbf{n}_x \times D_{xy} \mathbf{n}_y \varepsilon^\alpha) - i \mathbf{n}_x (\bar{\varepsilon} \psi_x \times \psi_x^\alpha) = 0 \\ \delta_{II}(\mathbf{n}_x^2) &= 2i \mathbf{n}_x (\mathbf{n}_x \times \bar{\varepsilon} \psi_x) = 0. \end{aligned} \quad (2.35)$$

We conclude that no nontrivial combination of the two transformations δ_I and δ_{II} can be a symmetry of the lattice theory, since the second transformation cannot restore the violation of the constraints caused by the first one. The second transformation on its own, however, can also not be a symmetry of the action because of $\{\mathcal{Q}_\alpha^{II}, \bar{\mathcal{Q}}_\beta^{II}\} = 2i\gamma_{\alpha\beta}^\mu \partial_\mu$. The superalgebra furthermore tells us that an approach based on a nilpotent supercharge is not possible, either, because such a nilpotent charge would have to be a combination of both supercharges and would hence violate the constraints.

Could we circumvent this restriction by improving the discretization in some way? Comparing our formulation with the one investigated in [13, 14], we see that the latter one contains an additional topological term. However, such a term does not affect the supersymmetry transformations (2.5) and (2.12) and hence cannot solve the problem. From a systematic point of view, there are only two modifications possible which are compatible with an $O(3)$ -invariant continuum limit. The first possibility is to modify the terms that are already present in the action. For example, one could introduce non-local interaction terms like $\sum_{x,y,z,w} C_{xyzw} (\bar{\psi}_x \psi_y) (\bar{\psi}_z \psi_w)$ instead of $\sum_x (\bar{\psi}_x \psi_x)^2$ [26]. The second possibility could be an inclusion of additional terms in the lattice action which vanish in the continuum limit. Any change of the action, however, does not have an impact on the constraints and hence cannot prevent their breaking. A modification of the constraints, by contrast, would directly alter the geometry of the target manifold and is thus no alternative. It follows that an improvement of the discretization could only maintain a part of supersymmetry by rendering the lattice action invariant under the second transformations. But this is not possible due to the structure of the superalgebra.

Even though these arguments were developed for a specific choice of coordinates, on finite lattices they also hold true for any reparametrization $(\mathbf{n}, \psi) \rightarrow (\mathbf{n}', \psi')$, because such a transformation

⁴Actually, it is also not a symmetry of the discretized action, but the breaking of the constraints is more severe.

is a bijective mapping between field values at a certain point x in spacetime, which commutes with discretization. As a consequence, one would observe the same pattern of symmetry breaking as depicted in (2.34) and (2.35). The single ambiguity that could arise here from the discretized derivative of the bosonic field is irrelevant since the presented arguments do not depend on the details of the lattice derivatives.

We conclude that it is just not possible to construct a discretization of the nonlinear $O(3)$ model which maintains $O(3)$ invariance as well as an exact supersymmetry. From this point of view, the symmetry breaking in the ansatz [13, 14] was inevitable. In this article we will work with the lattice formulation introduced in the previous section. It maintains the important $O(3)$ symmetry of the model while it breaks all supersymmetries. The latter should be restored in the continuum limit.

3 Numerical results

Before we present the results which are obtained by simulations for the $O(3)$ -symmetric lattice models described above, we want to demonstrate how a violation of the $O(3)$ symmetry arises in generic lattice formulations given in terms of unconstrained fields. We shall see that the symmetry of the continuum model is not recovered in the continuum limit.

3.1 Drawbacks of a \mathcal{Q} -exact lattice formulation

This problem can already be illustrated by investigating the bosonic $O(3)$ -NLSM. If we use a lattice derivative that is based on nearest neighbour interactions, the discretization of the bosonic part of (2.9) reads

$$S = \frac{2}{g^2} \sum_{\langle xy \rangle} \rho_{xy}^2 |\mathbf{u}_x - \mathbf{u}_y|^2. \quad (3.1)$$

At this point, an ambiguity in defining the density ρ_{xy}^2 arises. It must interpolate between ρ_x^2 and ρ_y^2 , which coincide in the continuum limit. Naively, many interpolations are feasible, e.g. one could use the arithmetic mean, $\rho_{xy}^2 = \frac{1}{2}(\rho_x^2 + \rho_y^2)$, or the geometric mean $\rho_{xy}^2 = \rho_x \rho_y$. In order to determine the appropriate interpolation one can apply the stereographic projection on the manifestly $O(3)$ invariant discretization in terms of the constrained \mathbf{n} -field and finds that ρ_{xy}^2 has to be implemented as the geometric mean.

To analyze a possible symmetry breaking in the formulation based on the arithmetic mean, simulations for both lattice prescriptions have been performed⁵ and it was tested if $\langle \bar{\mathbf{n}} \rangle = 0$ for $\bar{\mathbf{n}} = N^{-1} \sum_x \mathbf{n}_x$ in accordance with the global $O(3)$ symmetry, which cannot be spontaneously broken in two spacetime dimensions [27].

Fig. 4 shows that the discretization based on the geometric mean indeed yields $O(3)$ symmetric results whereas for the arithmetic mean only a $O(2)$ symmetry around the 1-axis remains. This is a direct consequence of the global $U(1)$ symmetry $u \rightarrow e^{i\phi} u$, where $u = u_1 + iu_2$. In the naive continuum limit both prescriptions are expected to coincide. In order to investigate this issue, simulations of the model based on the arithmetic mean have been carried out with different lattice sizes N and at different couplings g^{-2} . A restoration of the $O(3)$ symmetry implies a vanishing

⁵In the hybrid MC algorithm the factor ρ^2 of the path integral measure for the bosonic model, see (C.6), is absorbed in the action.

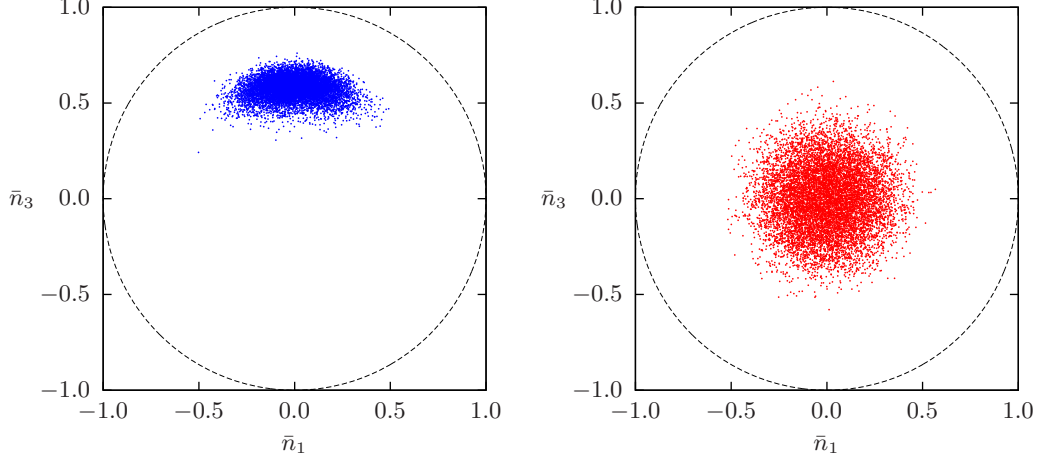


Figure 4. Scatter plot (projected to the \bar{n}_1 – \bar{n}_3 plane) of the averaged field \bar{n} for a lattice discretisation based on the arithmetic mean (left panel) and geometric mean (right panel) at $g^{-2} = 1$ and lattice size $N = 10 \times 10$.

$\langle \bar{n}_3 \rangle$ in the continuum limit. For a wide range of couplings $\langle \bar{n}_3 \rangle$ is independent of the lattice sizes such that the vacuum expectation value is assumed to be free of finite size effects (see Fig. 5, left panel). By fitting the correlator

$$C_B(t) = N_s^{-2} \text{Re} \sum_{x,y} \langle u_{(t,y)} \bar{u}_{(0,x)} \rangle \quad (3.2)$$

to $\cosh(ma(t - N_t/2))$ the mass $mL = maN_s$ measured in units of the physical box length can be extracted⁶. The analysis of $\langle \bar{n}_3 \rangle$ at fixed physical box size mL in the continuum limit (see Fig. 5, right panel) clearly shows that $\langle \bar{n}_3 \rangle$ grows to a value close to 1 for small lattice spacings, i.e. for large N and large g^{-2} . Therefore it is *impossible* to reach the correct $O(3)$ symmetric continuum limit for a regularization based on the arithmetic mean.

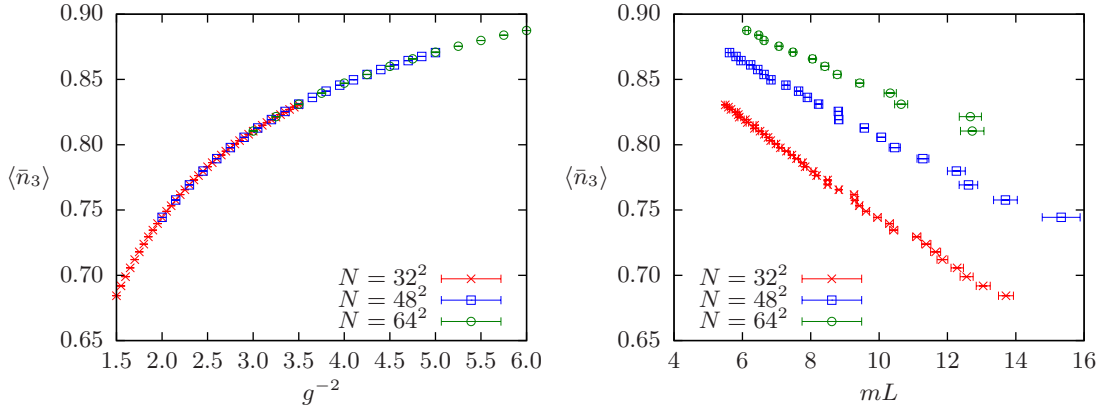


Figure 5. The value of $\langle \bar{n}_3 \rangle$ as indicator for a broken global $O(3)$ symmetry for three lattice volumes plotted over the coupling g^{-2} (left panel) and physical box size (right panel).

⁶Due to the $U(1)$ symmetry $\langle u \rangle = 0$, and $C_B(t)$ is the connected 2-point function.

Having encountered these problems in the simple bosonic case, we ought to be very careful with a discretization of the supersymmetric model and should always check the restoration of the $O(3)$ symmetry. Unfortunately this was not done in [13, 14] and we shall see below that this symmetry is actually broken in the lattice models constructed by Catterall and Ghadab.

The formulation in [13, 14] is based on a \mathcal{Q} -exact deformation of the $O(3)$ sigma model in the unconstrained \mathbb{CP}^1 formulation. The authors used Wilson fermions which break supersymmetry softly and showed that the \mathcal{Q} -based supersymmetry is restored in the continuum limit by studying the associated Ward identities. After performing a Hubbard-Stratonovich transformation to eliminate four-fermi terms the model contains two complex scalars u , σ and Dirac fermions Ψ . The path integral is

$$\mathcal{Z} = \int \mathcal{D}u \mathcal{D}\sigma \mathcal{D}\Psi \rho^{-2} e^{-S_B[u, \sigma] - S_F[u, \sigma, \Psi]} \quad \text{with} \quad (3.3)$$

$$S_B = \frac{2}{g^2} \sum_x \left(\rho_x^2 (\bar{\partial}^{\text{sym}} u)_x (\partial^{\text{sym}} \bar{u})_x + \rho_x^2 (\Delta u)_x (\Delta \bar{u})_x + \frac{1}{2} \sigma_x \bar{\sigma}_x \right), \quad (3.4)$$

where the symmetric derivative in direction μ is the arithmetic mean of the forward and backward derivatives, $\partial_\mu^{\text{sym}} = \frac{1}{2}(\partial_\mu^+ + \partial_\mu^-)$. The derivative operators without lower index denote the complex lattice derivatives $\partial = \partial_1 - i\partial_2$ and $\bar{\partial} = \partial_1 + i\partial_2$. The lattice Laplacian $\Delta = \sum_\mu \partial_\mu^+ \partial_\mu^-$ originates from the Wilson mass term in the fermionic action

$$S_F = \frac{2}{g^2} \bar{\Psi} M[u, \sigma] \Psi \quad (3.5)$$

with fermion matrix

$$M[u, \sigma] = \rho^2 \begin{pmatrix} \frac{1}{2}\Delta - \rho \bar{u}(\Delta u) + \text{h.c.} & \bar{\partial}^{\text{sym}} - 2\rho \bar{u}(\bar{\partial}^{\text{sym}} u) + \sigma \\ \partial^{\text{sym}} + 2\rho u(\partial^{\text{sym}} \bar{u}) - \bar{\sigma} & \frac{1}{2}\Delta - \rho \bar{u}(\Delta u) + \text{h.c.} \end{pmatrix}. \quad (3.6)$$

Periodic boundary conditions are assumed for *all fields* such that supersymmetry is not broken by the boundary conditions. The difference to a straightforward discretization is given by an *improvement term*

$$\Delta S = \frac{4}{g^2} \sum_x \rho_x^2 (\partial_1^{\text{sym}} u_2 \partial_2^{\text{sym}} u_1 - \partial_1^{\text{sym}} u_1 \partial_2^{\text{sym}} u_2) \quad (3.7)$$

which corresponds to the topological winding number and becomes irrelevant in the naive continuum limit, similar to the improvement term in the $\mathcal{N} = 2$ Wess-Zumino model [15]. For the simulation of this model on smaller lattices the HMC algorithm with an explicit calculation of the fermionic determinant is used. This has the advantage that no instabilities arise from introducing pseudo-fermions. Such instabilities may hide potential shortcomings of the lattice formulation.

The improvement term is analyzed for a lattice size of $N = 8 \times 8$ at coupling $g^{-2} = 1.5$. In our simulations a value of $S_B \approx 2N$ is found (with statistical fluctuations of about 10%) in agreement with the simplest Ward identity [14], which is a consequence of the (nearly, up to the Wilson mass) lattice supersymmetry. In Fig. 6 the MC histories of \bar{n}_3 and ΔS are plotted and they shed light on the influence of the improvement term on the dynamics. At a certain point in the simulation the value of \bar{n}_3 freezes out and the improvement term starts growing largely negative. Just as for the Nicolai improved Wess-Zumino model [15] the lattice system is driven away from the continuum

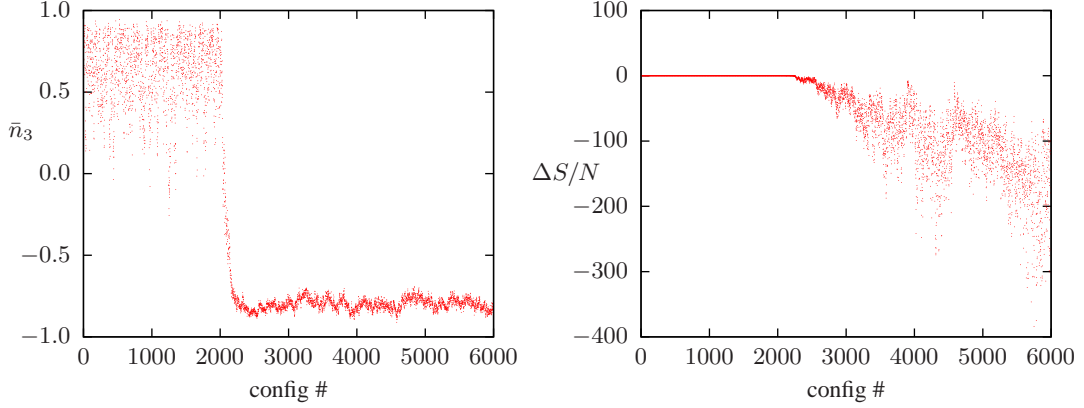


Figure 6. MC history of \bar{n}_3 (left panel) and ΔS (right panel) for a simulation of the lattice model (3.3) at coupling $g^{-2} = 1.5$ on an 8×8 lattice.

physics, where ΔS must vanish, into an unphysical phase⁷. We conclude that the known problems of improved actions must be taken into account also in simulations of supersymmetric sigma models – only configurations from the physical phase with nearly vanishing improvement term should be taken into account in measurements. Tunnel events to the unphysical phase are suppressed on large lattices and weak coupling g , i.e. in the continuum limit, similarly as for Wess-Zumino models. Nevertheless, these observations suggest that similar problems may arise in simulations of all lattice models with exact supersymmetry that are constructed from a \mathcal{Q} -exact action, e.g. two dimensional $\mathcal{N} = 2$ Super Yang-Mills [28].

But why did this instability not show up in the results of [14]? The answer may be that in the rational HMC algorithm used in the simulations spectral bounds must be chosen to cover the spectrum of $M^\dagger M$. Typically these are obtained by test runs with rather pessimistic bounds and *small statistics*, such that only the physical phase with $\Delta S \approx 0$ is present. But for the simulation that is shown in Fig. 6 the lowest eigenvalue of $M^\dagger M$ decreases by a factor of 10^{-5} when entering the unphysical phase.⁸ For that reason the rational hybrid Monte-Carlo algorithm with spectral bounds that are not applicable to the whole simulation will be an *inexact* algorithm and will give an arbitrarily small acceptance rate for the unphysical configurations that dominate the path integral. Furthermore $\text{sign det } M$ is not positive definite and a *deflated* rational hybrid Monte-Carlo algorithm is necessary to get reliable expectation values.

These results imply that for a reliable measurement of $\langle \bar{n}_3 \rangle$ large g^{-2} must be used in order to suppress the unphysical phase. Since the continuum limit is reached for $g \rightarrow 0$, measurements will be affected by finite size corrections. The corrections of the observable \bar{n}_3 are assumed to vanish exponentially with growing volume,

$$\langle \bar{n}_3 \rangle (N_s) = \langle \bar{n}_3 \rangle (\infty) + A e^{-B N_s}, \quad (3.8)$$

such that a fit to this functional form for $N_s \in \{10, 11, 12, 13, 14, 16\}$ and corresponding lattice volumes $N = N_s^2$ reveals the infinite volume value for $g^{-2} \in \{3.5, 4.0, 4.5, 5.0\}$, see Fig. 7 (left panel). Although $\langle \bar{n}_3 \rangle$ decreases for fixed N_s and growing g^{-2} , the infinite volume values tend to

⁷The normalized improvement term $\Delta S/N$ fluctuates around zero with a width of about 0.002 in the physical phase.

⁸The largest eigenvalue of $M^\dagger M$ is kept at the same order of magnitude in the unphysical phase.

grow for larger g^{-2} , see Fig. 7 (right panel). Therefore the $O(3)$ symmetry will *not* be restored in the infinite volume continuum limit of the lattice model (3.3). All these results have a crucial

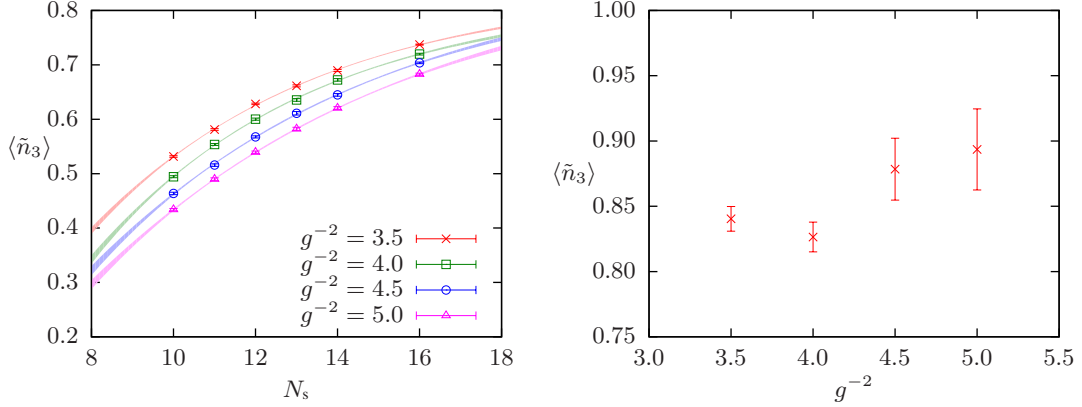


Figure 7. Left panel: $\langle \tilde{n}_3 \rangle$ for different lattice volumes $N = N_s^2$ at four couplings g^{-2} . The infinite volume extrapolation according to Eq. (3.8) is indicated by the shaded areas. Right panel: Infinite volume values of $\langle \tilde{n}_3 \rangle$ for different g^{-2} .

implication. Although the formulation (3.3) may restore the full $\mathcal{N} = (2, 2)$ supersymmetry on the lattice, the resulting continuum model is *not* the supersymmetric $O(3)$ model, because the global $O(3)$ symmetry, that cannot be broken spontaneously in the continuum model [27], is *not restored* in the continuum limit.

3.2 $O(3)$ symmetric formulations

The previous studies have stressed the importance of an $O(3)$ invariant formulation of the theory. The discretizations given in section 2.3 respect the global flavor symmetry and in order to check whether the corresponding algorithms respect it as well we record the expectation value of \mathbf{n} . For the coset construction with group valued field R the expectation value vanishes and the autocorrelation times are small. For the stereographically projected fields \mathbf{u} we generate $O(3)$ symmetric configurations but observe large autocorrelation times for observables which depend on the field component corresponding to the projection axis. This stems from the interplay between stereographic projection and molecular dynamics steps which introduce two pseudo-momenta and a pseudo-Hamiltonian for \mathbf{u} to generate test configurations. Computing the pseudo-momenta for the constrained variables, we see that the momentum corresponding to the projection axis used in the HMC algorithm takes values roughly one half of the other momenta. In the language of unconstrained variables, evolution of configurations is glued to a hyperplane of constant \mathbf{u}^2 , which can be seen from figure 8 (left panel), where \mathbf{u}^2 , \mathbf{v}^2 and \mathbf{w}^2 correspond to the three possible (canonical) projection axes, while the actual projection axis of the HMC algorithm is fixed. To circumvent this problem, the projection axis in the molecular dynamics step is changed repeatedly between successive trial and acceptance steps. While it is in principle possible to choose random projection axes for every update, we rotate through the three canonical axes, saving only every third configuration which corresponds to a fixed projection axis. A Metropolis acceptance step is yet needed after each change of the projection axis. The right panel of figure 8 illustrates how this improved

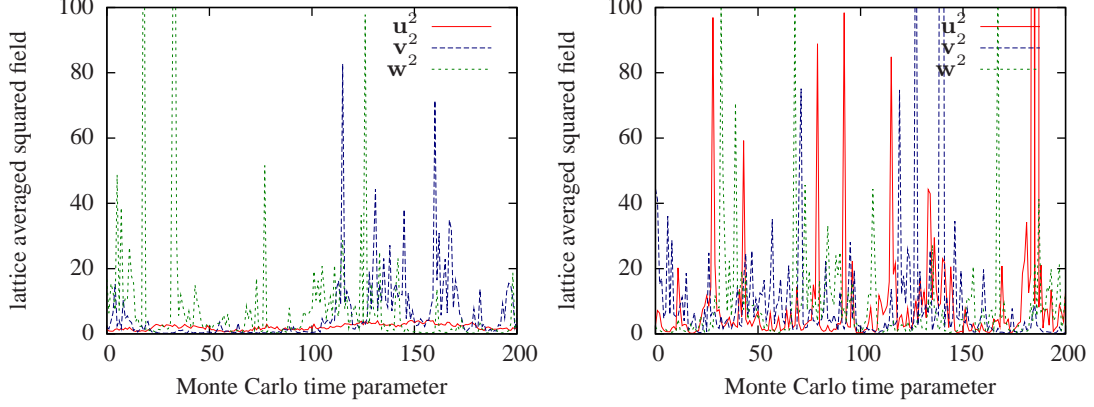


Figure 8. MC-histories for the lattice averages of u^2 , v^2 and w^2 using the three different projection axes in the usual HMC algorithm (left panel) and the improved algorithm (right panel). Note that fluctuations for u^2 which corresponds to the projection axis chosen in the HMC algorithm are severely suppressed in the left panel.

update scheme restores the balance between the three projection axes. The configuration space is traversed quickly and the expectation values $\langle n_i \rangle$ decrease with ongoing MC time.

3.3 Fermionic masses

The classical theory has no intrinsic mass scale. But there is a relation between mass gap and bare coupling by dimensional transmutation. In the $\overline{\text{MS}}$ scheme it is possible to compute the mass gap [8, 29] in relation to $\Lambda_{\overline{\text{MS}}}$. Investigations of the $\mathcal{N} = 1$ Wess-Zumino model have revealed that the fermionic mass is less affected by finite size effects than the bosonic mass. For that reason the fermionic mass is used to set the physical scale of the lattice, i.e. the lattice spacing and the physical box length. The $O(3)$ symmetric fermionic correlator for group-valued fields is constructed as

$$\begin{aligned}
 \langle i\bar{\psi}_x \psi_y \rangle &= Z^{-1} \int \mathcal{D}\mathbf{n} \mathcal{D}\sigma \mathcal{D}\psi \delta(\mathbf{n}\psi) \delta(\mathbf{n}^2 - 1) (i\bar{\psi}_x \psi_y) e^{-S} \\
 &= Z^{-1} \int \mathcal{D}R \mathcal{D}\sigma e^{-S_B} \int \mathcal{D}\chi \ i\bar{\chi}_x \kappa^\top R_x^\top R_y \kappa \chi_y e^{-S_F} \\
 &= g^2 \left\langle \text{tr}_{f,s} (R_x \kappa C Q_{xy}^{-1} \kappa^\top R_y^\top) \right\rangle, \quad \kappa^\top = \begin{pmatrix} 0 & 1 & 0 \\ 0 & 0 & 1 \end{pmatrix},
 \end{aligned} \tag{3.9}$$

with S_F given in (2.21) and ‘ $\text{tr}_{f,s}$ ’ indicates the trace over flavor and spinor indices. The corresponding timeslice correlator is given by $C_F(t) = N_s^{-2} \sum_{xy} \langle i\bar{\psi}_{(t,x)} \psi_{(0,y)} \rangle$. In order to measure the mass in *one* of the ground states the configurations are projected, without loss of generality, onto the sector with $\Xi > 0$ for $a\Xi = N^{-1} \sum_x \bar{\psi}_x \psi_x$. This can be achieved by flipping the sign of σ for configurations with $\Xi < 0$. Using these definitions the fermionic masses are obtained by a cosh fit to the correlator over the range $t \in]0, N_t[$. A similar procedure is utilized in the case of stereographically projected fermions, where we have to use the projected fermion correlator instead

of (3.9),

$$\begin{aligned}\langle i\bar{\psi}_{x,\perp}\psi_{y,\perp}\rangle &= \langle 4\rho_x i\bar{\lambda}_x \lambda_y \rho_y - 8\rho_x (u_x i\bar{\lambda}_x)(\lambda_y u_y) \rho_y^2 - 8\rho_x^2 (u_x i\bar{\lambda}_x)(\lambda_y u_y) \rho_y \\ &\quad + 16\rho_x^2 (u_x i\bar{\lambda}_x)(u_x u_y)(\lambda_y u_y) \rho_y^2 \rangle, \\ \langle i\bar{\psi}_{x,1}\psi_{y,1}\rangle &= \langle 16\rho_x^2 (u_x i\bar{\lambda}_x)(\lambda_y u_y) \rho_y^2 \rangle.\end{aligned}\quad (3.10)$$

In this case non-diagonal elements contribute to the full correlator, which relate unconstrained fields of different flavor. A comparison of the fermionic masses for different lattice sizes using the SLAC derivative (see Figure 9) reveals that finite size effects on $m_F a$ are within statistical error bars if $m_F L \gtrsim 5$.

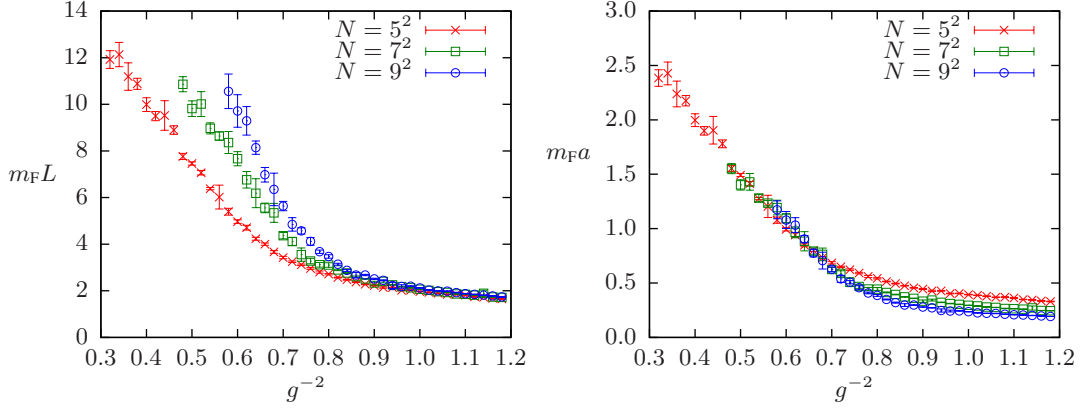


Figure 9. Fermionic masses from SLAC ensembles in units of the box length (left panel) and lattice spacing (right panel) for different lattice volumes and bare couplings g^{-2} computed using up to $2 \cdot 10^7$ configurations.

3.4 Chiral symmetry breaking

Due to the orthogonality of R_x the chiral condensate in the coset formulation simplifies to

$$\langle i\bar{\psi}_x \psi_x \rangle = Z^{-1} \int \mathcal{D}R \mathcal{D}\sigma e^{-S_B} \int \mathcal{D}\chi i\bar{\chi}_x \chi_x e^{-S_F} = g^2 \langle \text{tr}_{f,s}(CQ_{xx}^{-1}) \rangle. \quad (3.11)$$

Using stereographic projection, however, we have to compute the projected condensate given in terms of unconstrained fields. This is obtained by using the trace of the correlator given in equation (3.10). If we rewrite the action (2.17) as $S = S_B[u, \sigma] + \lambda^\top P \lambda$, we can replace the quadratic fermion operator by

$$\langle \dots \bar{\lambda}_{x,i} \lambda_{y,j} \dots \rangle = \langle \dots C(P^{-1})_{xy,ij} \dots \rangle. \quad (3.12)$$

The continuum model is invariant under a discrete chiral symmetry $\psi \rightarrow i\gamma_* \psi$. It is spontaneously broken in the infinite volume limit and the supersymmetric ground states correspond to the two ground states of this broken symmetry [30]. A discretization based on the SLAC derivative maintains chiral symmetry on the lattice by the cost of having a non-local derivative. For every finite lattice volume the expectation value $\langle i\bar{\psi}\psi \rangle$ will vanish and is hence not the appropriate measure to trace a broken symmetry. One should instead analyze the histograms of the volume average

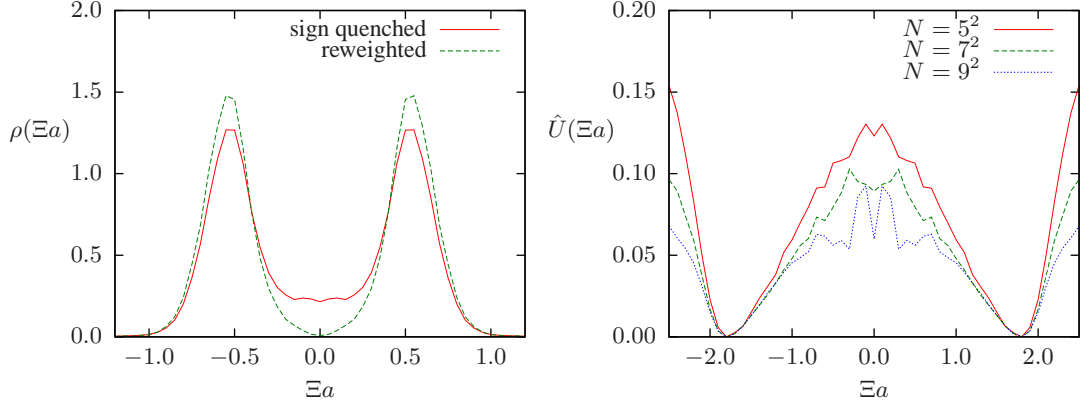


Figure 10. Left panel: Probability density of the volume averaged chiral condensate for lattice size 9×9 at a bare coupling $g^{-2} = 1$ in the sign quenched and reweighted ensemble using the SLAC derivative. Right panel: Constraint effective potential (normalised to $\min_{(a\Xi)} \hat{U}(a\Xi) = 0$) of the chiral condensate for different lattice volumes at $g^{-2} = 0.64$ computed using up to $3 \cdot 10^7$ configurations and the SLAC derivative.

$a\Xi = N^{-1} \sum_x \bar{\psi}_x \psi_x$. Fig. 10 (left panel) clearly shows a double peak structure of the corresponding distribution $\rho(a\Xi)$, coinciding with the two ground states. The reweighting process reveals that a cancellation between positive and negative Pfaffians happens mostly for $a\Xi \approx 0$. In the analysis of the constrained effective potential $\hat{U}(a\Xi) = -\ln(\rho(a\Xi))/N$ for several lattice volumes at fixed coupling (see Fig. 10, right panel) no running of the two minima is visible, such that there will be a spontaneous chiral symmetry breaking in the infinite volume limit of the lattice model.

3.5 Bosonic masses

In order to test whether the chosen discretization corresponds to a supersymmetric theory, one should check the degeneracy of the bosonic and fermionic masses. The bosonic masses $m_B L$ are extracted from the $O(3)$ invariant correlator (2.31) via a cosh fit over the range $t \in]0, N_t[$. The bosonic correlator is unaffected by a change in σ , such that no projection on one of the two ground states is necessary. Having computed the boson masses, we can compare them with the fermionic ones for different couplings and lattice sizes.

Simulations using SLAC fermions Calculations have been performed on lattice sizes $N \in \{5^2, 7^2, 9^2\}$ over a coupling range $g^{-2} \in [0.4, 1.2]$. The direct comparison is shown in Fig. 11 (left panel) and the results seem to be disappointing at first sight. The bosonic masses lie considerably below the fermionic partners and this deviation becomes even more pronounced for larger lattices. However, this does not necessarily imply that supersymmetry will be broken in the continuum limit. Already for the simple lattice $\mathcal{N}=2$ Wess-Zumino model with spontaneously broken \mathbb{Z}_2 symmetry and one exact supersymmetry the masses split in the strong coupling regime at finite physical box sizes [15]. E.g. for couplings for which the one-loop perturbation theory fails and for a box size $m_F L \approx 10$, a 20% splitting with a smaller bosonic mass is observed. From that point of view the supersymmetric $O(3)$ nonlinear sigma model could be similar to a strongly coupled $\mathcal{N} = 2$ Wess-Zumino model. The finite size effects may be even larger and a mass splitting of

much more than 20% would not be surprising for $m_F L < 10$. Only an analysis of the mass ratio m_B/m_F in the large volume limit can uncover a restoration of degenerate masses. This is exemplarily shown for the results on the 5×5 lattice in Fig. 11 (right panel). Despite the fact that lattice artefacts are sizeable the basic mechanism becomes clear. In the limit of large volumes a relation

$$m_B L = m_F L - \Delta M \quad \Rightarrow \quad \frac{m_B}{m_F} = 1 - \frac{\Delta M}{m_F L} \quad (3.13)$$

with constant ΔM is found, such that the ratio tends to 1 and the masses will be degenerate in the infinite volume limit.⁹

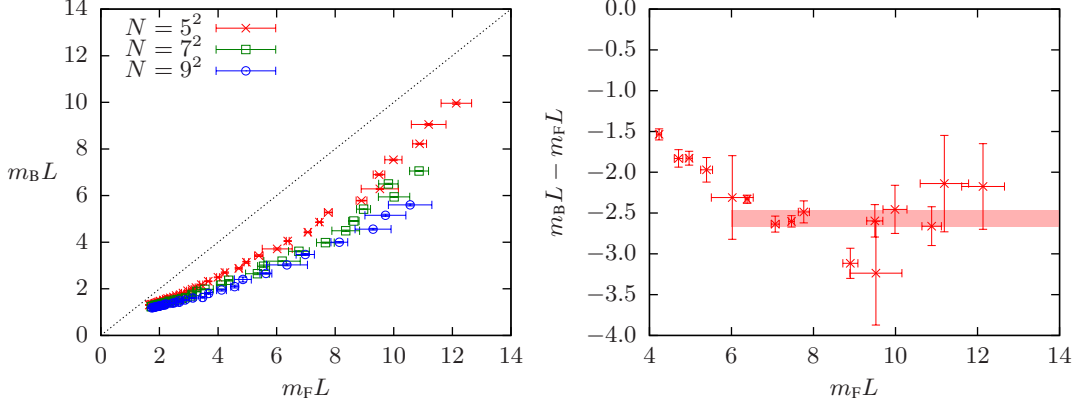


Figure 11. Left panel: Direct comparison of bosonic and fermionic mass from the SLAC ensemble in units of the box size for three different lattice sizes. The dotted line denotes the case $m_F = m_B$. Right panel: Difference $m_B L - m_F L$ for varying box size $m_F L$ on a 5×5 lattice. The shaded area denotes a fit according to Eq. (3.13) for $m_F L > 6$.

But the accessible physical volumes at larger lattices still do not allow for a reliable extrapolation of the corresponding ΔM and no continuum limit can be taken at the moment. It is hence an open question if eq. (3.13) also holds true in the continuum limit and if supersymmetry will be restored. These questions should be resolved by computations on larger lattices. Such computations, however, become unfeasible because of the sign problem, which worsens with increasing lattice size in case of the SLAC derivative, see appendix D. Nevertheless, further information about the supersymmetric features of the implementation can be obtained by studying a corresponding Ward identity, cf. section 3.7.

Simulations using Wilson fermions While the applicability of the SLAC derivative is confined to small lattice volumes due to the strong sign problem, Wilson fermions offer the possibility to explore larger volumes by utilizing efficiently preconditioned pseudofermion algorithms (compare to appendix E), however at the cost of larger lattice artifacts. Bosonic masses are extracted as explained beforehand by calculating the stereographically projected correlators

$$\begin{aligned} \langle n_{x,\perp} n_{y,\perp} \rangle &= 4 \langle \rho_x u_x u_y \rho_y \rangle, \\ \langle n_{x,1} n_{y,1} \rangle &= \langle \rho_x (1 - u_x^2) (1 - u_y^2) \rho_y \rangle. \end{aligned} \quad (3.14)$$

⁹For the 5×5 lattice a fit to Eq. (3.13) for $m_F L > 6$ gives $\Delta M = 2.56(10)$.

For lattice volumes up to 32^2 we obtain a discrepancy between bosonic and fermionic masses with lighter bosons, see Figure 12. This gap increases for larger lattices and there is no indication of a degeneracy in the continuum limit, so that supersymmetry is seemingly not restored. This is not too surprising, though, since Wilson fermions may break supersymmetry in a way that is not dissolved in the continuum limit.

In section 2.5 we showed that it is not possible to construct a discretized action which simultaneously respects at least one exact supersymmetry as well as the $O(3)$ symmetry. An improved action thus relies on adding fine tuning terms as a compensation for renormalized couplings that arise from symmetry breaking terms on the lattice.

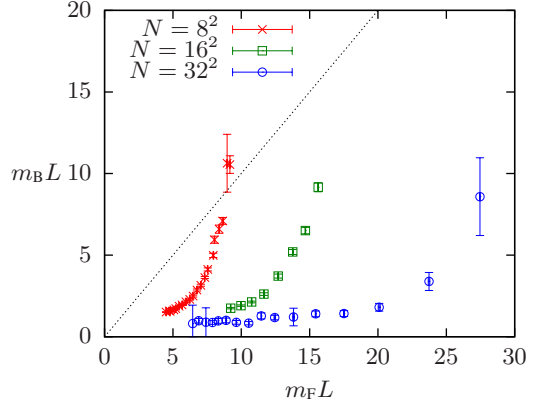


Figure 12. Comparison of bosonic and fermionic mass in units of the box size for three different lattice sizes using Wilson fermions. The dotted line denotes the case $m_F = m_B$.

3.6 Fine tuning of the Wilson derivative

From $\mathcal{N}=1$ Super Yang-Mills theories it is known that the correct continuum limit may be achieved by a fine tuning term that resembles an explicit fermionic mass such that the renormalized gluino mass is zero [31]. A similar procedure will be performed in the present case by deforming the fermionic derivative using a fine tuning mass m ,

$$M_{xy}^{\alpha\beta} = \gamma_\mu^{\alpha\beta} (\partial_\mu^{sym})_{xy} + \delta^{\alpha\beta} \frac{ra}{2} \Delta_{xy} + \delta^{\alpha\beta} m \delta_{xy}, \quad (3.15)$$

which enters the Hopping parameter $\kappa = (4 + 2m)^{-1}$. Additional degrees of freedom in the fine tuning procedure increase the numerical effort considerably, such that a careful choice of tuning parameters is necessary in order to keep the RHMC algorithm exact and efficient. In particular, for different κ , we have monitored the sign of the Pfaffian determinant as well as the spectrum of the Dirac operator, which is approximated by rational functions [32]. To guide our efforts, we measure the chiral condensate, bosonic and fermionic masses as well as the bosonic action for several values of the fine tuning parameter.

The chiral condensate is extracted from the trace of the projected correlator, as described in (3.10), while the sign of the Pfaffian is taken into account by a reweighting procedure,

$$\langle \bar{\psi} \psi \rangle = \frac{\langle \text{sgn Pf } \bar{\psi} \psi \rangle_q}{\langle \text{sgn Pf} \rangle_q}. \quad (3.16)$$

Here, $\langle \dots \rangle_q$ denotes the sign-quenched ensemble. For the Wilson derivative we expect that one of the ground state energies is raised due to the explicit breaking of chiral symmetry, so that we get fluctuations around one of the minima in Figure 10 only. Switching on the fine tuning mass, the condensate is driven to larger values, showing a jump at some distinct point (see Figure 13, left panel). To gain a better understanding of this behaviour, we utilize histograms of the chiral

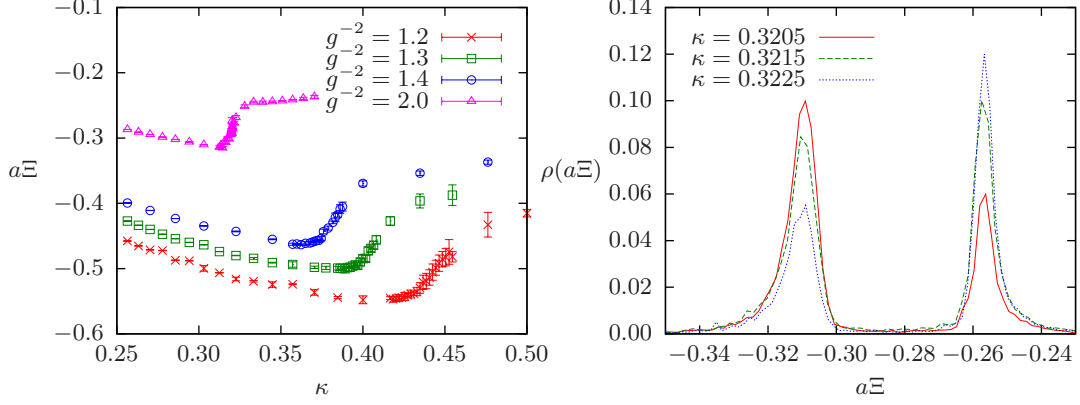


Figure 13. Left Panel: Expectation value of the chiral condensate $a\Xi$ for lattice volume 16^2 and different couplings g^{-2} . A jump corresponding to a first order transition is visible. Right Panel: Histograms of the chiral condensate $a\Xi$ for different values of the Hopping parameter ($N = 24^2$, $g^{-2} = 2$).

condensate to measure the distribution function $\rho(a\Xi)$, which is formally obtained by introducing a delta function into the partition sum,

$$\rho(a\Xi) = \frac{1}{Z} \int \mathcal{D}n \mathcal{D}\psi \delta(a\Xi - i\bar{\psi}\psi) e^{-S} \longrightarrow \frac{1}{M} \sum_{i=1}^M \delta(a\Xi - i(\bar{\psi}\psi)_i).$$

It is henceforth possible to express the expectation value for the chiral condensate using this quantity as $\langle i\bar{\psi}\psi \rangle = \sum_{i=1}^M a\Xi_i \rho(a\Xi_i) / \sum_{i=1}^M \rho(a\Xi_i)$. Simulating the sign-quenched ensemble, we need to use the reweighted distribution function,

$$\rho(a\Xi) = \frac{1}{M} \sum_{i=1}^M \delta(a\Xi - i(\bar{\psi}\psi)_i) \frac{\text{sgn Pf}_i}{\langle \text{sgn Pf} \rangle_q}, \quad (3.17)$$

which may no longer be interpreted as a probability distribution, since sgn Pf can be negative. In contrast to the case of SLAC fermions, where no problem arises due to intact \mathbb{Z}_2 -symmetry, the Wilson prescription leads to an additive renormalization, such that configurations with negative sign yield entries corresponding to a sign-flipped renormalization constant. To avoid this behaviour, we will omit the sign information when considering histograms, seeing that the Wilson ensemble shows frequent sign fluctuations only in the direct vicinity of the critical Hopping parameter and therefore allows to extrapolate from a region where omitting the sign is safe. Expectation values are however *always* determined using the reweighting procedure and are hence not affected by this approximation. By an appropriate choice of the tuning parameter

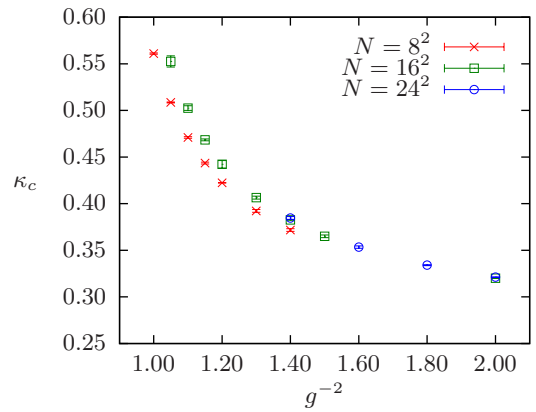


Figure 14. Critical value of the Hopping parameter for several lattice sizes.

we obtain the spontaneously broken signature that is expected in the continuum limit (see Figure 13, right panel), modified by the additive renormalization. The point of steep increase is identified as a first order phase transition in the chiral condensate, which is analogous to the case of Super-Yang-Mills theories. Using this signature, we have determined the critical value of the fine tuning parameter κ for lattice sizes 8^2 , 16^2 and 24^2 and coupling $g^{-2} = 1 \dots 2$, see Figure 14.

Regarding the masses of the elementary excitations, we see that the bosonic correlator is not affected by the fine tuning procedure and the bosonic mass takes a constant value within error bars. For the fermionic mass, we observe linear scaling behaviour for $\kappa < \kappa_c$ and $\kappa > \kappa_c$, however in the vicinity of $\kappa \approx \kappa_c$, the scaling breaks down (Figure 15, left panel). Therefore, a reliable extrapolation of the fermionic mass based on small values of κ is not possible, at least for the lattice volumes considered. We will hence utilize the bosonic mass to fix the physical box size $m_B L$ for our investigations involving fine tuning. In contrast to e.g. $\mathcal{N}=1$ Super Yang-Mills [31], simulations at the critical point are feasible since the theory inhibits a finite mass gap even in the continuum. In the vicinity of the phase transition, mixing between the two ground states occurs and

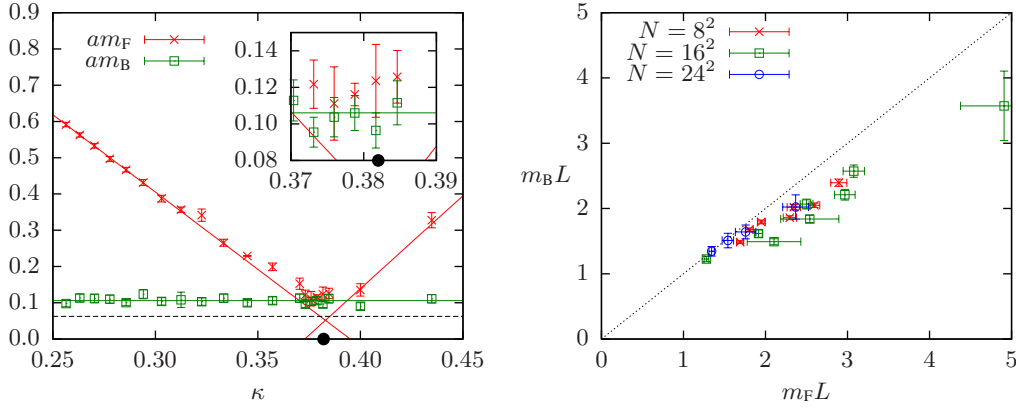


Figure 15. Left Panel: Scaling behaviour of the bosonic and fermionic mass for $N = 16^2$ and $g^{-2} = 1.4$ with $\kappa_c = 0.382(1)$, marked by the black dot. The dashed line denotes the lattice cutoff of $1/16$. Right Panel: Comparison of bosonic and fermionic masses in units of the box size for three different lattice sizes at $\kappa = \kappa_c$.

the $i\bar{\psi}\psi$ correlator must be projected onto one of the ground states, analogously to the SLAC case (see chapter 3.3). However, since we may only determine the additive renormalization constant from the chiral condensate distribution function up to finite precision, fermion mass extraction is affected by a systematic error which comes from configurations with close to vanishing renormalized chiral condensate that are erroneously weighted as belonging to the false ground state. This error is negligible for large lattices and g^{-2} though, since these configurations are suppressed by the finite tunneling probability between both ground states. We observe a great improvement regarding the degeneracy of the masses (Figure 15, right panel), which is expected in the continuum limit from supersymmetry restoration. In particular, the fermionic masses no longer “run away” if the volume is increased, which hints at a proper cancellation of the divergent operator causing these problems (compare to Figure 12). Nevertheless, a true proof of this conjecture may only be provided by a study of all divergent operators based on lattice perturbation theory, which is not pursued here. For finite box sizes of $m_F L > 2$ a thermal mass-splitting similar to the SLAC case

seems to emerge, however showing a slightly smaller gap. To explore this region, further large volume simulations would be needed in order to suppress lattice artifacts.

3.7 Path integral based Ward identity

Similar to the Ward identity that is given in [14] an equivalent relation can be derived for the present lattice model. Starting from the path integral in the continuum, Q exactness is given by the twisted supercharge [14] in the continuum, such that $S = \frac{1}{2g^2} Q\Lambda$ with $Q^2 = 0$. This implies the continuum Ward identity

$$\frac{\partial \ln \mathcal{Z}}{\partial(g^{-2})} = \langle -\frac{1}{2} Q\Lambda \rangle = 0, \quad (3.18)$$

since action and measure are invariant under the symmetry transformation generated by Q . After putting the theory on the lattice, integrating out the constrained auxiliary field f , and introducing the unconstrained field σ to get rid of the four-fermion interaction (in that order) one is left with the path integral,

$$\mathcal{Z} = g^N \int D R D \sigma D \lambda e^{-S[R, \sigma, \lambda]} \quad (3.19)$$

with N as number of lattice sites and the action given in eq. (2.20).¹⁰ Here, the coupling dependent part is important, so that only constant numerical factors may be dropped. The derivative of the Schwinger functional is

$$\frac{\partial \ln \mathcal{Z}}{\partial(g^{-2})} = -\frac{Ng^2}{2} - g^2 \langle S_B \rangle + g^2 \frac{\dim Q_F}{2}, \quad (3.20)$$

where Q_F denotes the Dirac operator in (2.22), and $\dim Q_F$ is its dimension in terms of flavor and spinor components as well as lattices sites. In our case the Ward identity (3.18) reads

$$\langle S_B \rangle = \frac{3}{2} N, \quad (3.21)$$

with S_B defined in Eq. (2.21). The same Ward identity can be derived for the formulation based on the stereographic projection.

In order to see a possible restoration of supersymmetry in the continuum limit, the bosonic action has been calculated with the SLAC derivative for three lattice sizes in a coupling range where finite size effects should be negligible, i.e. for $m_F L > 5$. The results that are shown in Fig. 16 (left panel) reveal that for the smallest (5×5) lattice Eq. (3.21) is violated as much as 10% for $m_F L \approx 5$ and up to 20% at $m_F L \approx 10$. Therefore the Ward identity violation grows for coarser lattice spacings. However, in the continuum limit at a fixed physical volume $m_F L$ the Ward identity tends to be restored, cf. Fig 16 (left panel). Additionally one can explore the small volume regime of this theory by sending $g \rightarrow 0$ at fixed lattice volume to reach the continuum limit. This has been performed on a 7×7 lattice for a large range of couplings $g^{-2} \in [0.4, 100]$, see Fig. 16 (right panel). Here the Ward identity is explicitly restored in the limit of large g^{-2} , although this result has to be taken with care since the physical box size becomes unreliably small.

The examined lattice sizes are rather small, but these observations at least imply that a supersymmetric continuum limit can be reached and that the non-degeneracy of bosonic and fermionic mass

¹⁰The factor g^N in front of the path integral stems from the Gaussian integrals that need to be carried out for f and be introduced for σ .

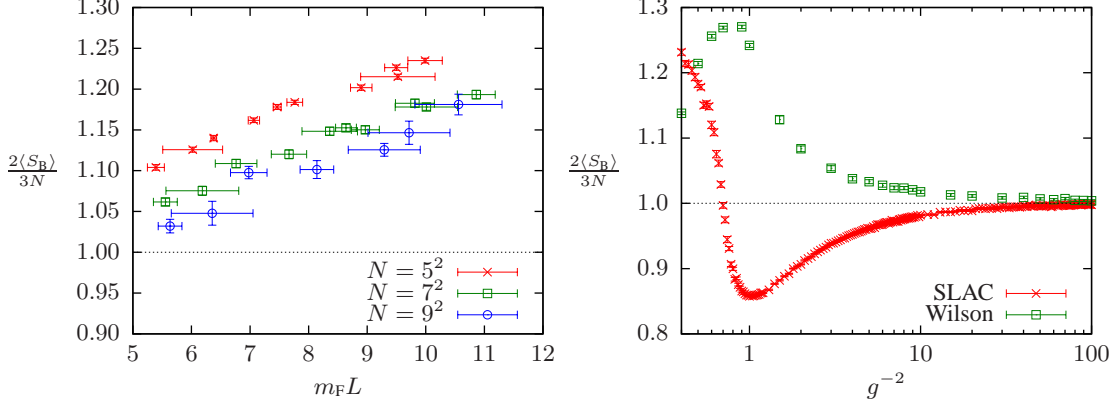


Figure 16. Normalized action $2\langle S_B \rangle / 3N$, which will take the value 1 if supersymmetry is restored in the continuum limit as required by the Ward identity (3.21). Left panel: Measurements for different lattice sizes with physical volumes $5 < m_F L < 11$ in the SLAC ensemble. Right panel: Results for fixed lattice volume $N = 7^2$ (SLAC) and $N = 8^2$ (Wilson, $\kappa = 0.25$ fixed) and couplings $g^{-2} \in [0.4, 100]$ that reach the regime of small physical volumes (small g).

is a finite size effect. However, in order to obtain a definite answer simulations on larger lattices would be necessary. For instance, one ought to verify that $\langle S_B \rangle / N$ does not undershoot and drop below 1.5 in the continuum limit at fixed $m_F L$. Using the Wilson derivative, we measured the bosonic action in the finetuned ensemble at $\kappa = \kappa_c$ and observe similar behavior, although for the largest lattice considered we see a discrepancy of 7% for fine lattice spacing ($g^{-2} = 2$) and up to 14% for a coarser lattice spacing ($g^{-2} = 1.4$), see figure 17. However, unlike for SLAC fermions, the Ward identity approaches its continuum value from above in the limit of g^{-2} to infinity and therefore is unlikely to undershoot (see Fig. 16, right panel). Hence a comparison of both derivatives is only valid in the regime of large g^{-2} where monotonic behaviour is encountered, which is however unavailable for the SLAC derivative due to either fine-size effects for small lattices or the strong sign problem for large lattices. Overall, the slope of the Ward identity clearly points to a restoration of supersymmetry in the continuum limit.

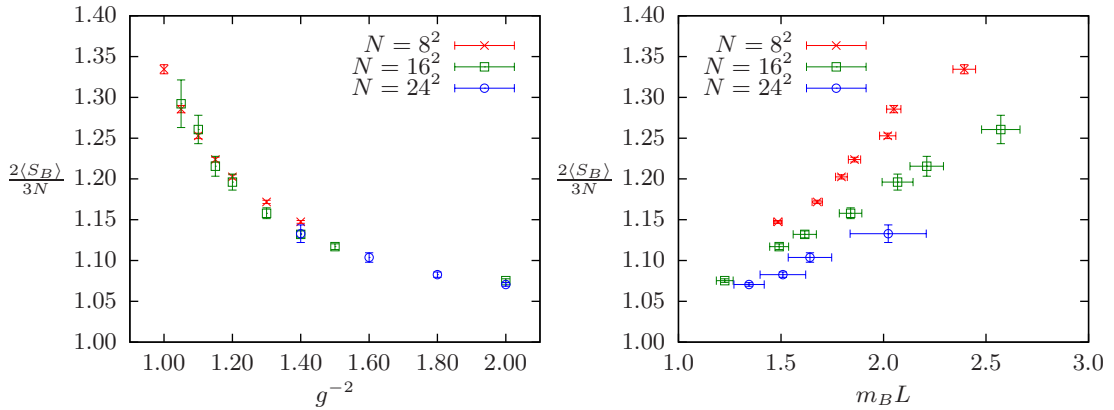


Figure 17. Expectation value of the bosonic action at $\kappa = \kappa_c$ for different g^{-2} (left panel) and different box sizes (right panel). $\frac{2\langle S_B \rangle}{3N} = 1$ is expected in the supersymmetric continuum limit.

4 Conclusion

The purpose of this article was to obtain a lattice formulation of the supersymmetric nonlinear $O(3)$ model which maintains the symmetries of the theory, at least in the continuum limit. The target manifold of the model is Kähler and hence it possesses an $\mathcal{N} = 2$ supersymmetry, which could provide for a nilpotent supercharge and a discretization prescription based on this which maintains an exact supersymmetry on the lattice. We first derived the supersymmetry transformation in terms of constrained field variables and used these to analyze the applicability of such an approach in the nonlinear $O(3)$ model. We realized that there is in fact no way to formulate a discretization of the theory which maintains simultaneously both the $O(3)$ symmetry and a part of supersymmetry. We explicitly verified that the Q -exact supersymmetric formulation presented in [14] breaks the $O(3)$ symmetry such that it is not restored even in the continuum limit.

In contrast, we started from a manifestly $O(3)$ symmetric discretization and investigated whether the supersymmetry is restored in the continuum limit. The spherical geometry of the target space is treated by two separate approaches, group valued variables on the one hand and a stereographic projection on the other hand. The numerical simulations are performed with the SLAC derivative and the Wilson derivative respectively. The former does not break the chiral \mathbb{Z}_2 symmetry of the classical action explicitly, allowing for the evaluation of histograms to verify the symmetric ground state structure which is spontaneously broken. The applicability of the SLAC derivative in theories with curved target space was illustrated by a calculation of the step scaling function in the quenched model. A disadvantage of the SLAC derivative, however, is the strong sign problem that becomes relevant already at comparably small lattices. In a sense the SLAC derivative is already too close to the continuum limit since it correctly reflects the intrinsic sign problem even on moderately sized lattices. In order to test the supersymmetric properties of our lattice models we analyzed the masses of fermions and bosons as well as a Ward identity based on the bosonic action. For both derivatives the results indicate that the Ward identity is fulfilled in the continuum limit at finite (large) physical volume. Concerning the expected degeneracy of the masses, no final statement can be done based on the small lattice sizes that are accessible by the SLAC derivative. The Wilson derivative enables us to investigate larger lattices, but breaks chiral symmetry explicitly at finite lattice spacing, which leads to the renormalization of relevant operators in such a way that one is carried away from the supersymmetric continuum limit. Motivated by Super Yang-Mills theory, we fine tuned the fermionic mass in order to remove the explicit breaking of the chiral symmetry. Furthermore, using the thus tuned ensemble, no "run away" of fermionic masses is visible, but rather a degeneracy of boson and fermion masses. This indicates that a single parameter is sufficient to provide for a supersymmetric continuum limit and for a cancellation of the encountered divergences. This, however, remains a conjecture until explicitly checked by means of lattice perturbation theory.

We have therefore presented a lattice discretization which incorporates the $O(3)$ symmetry exactly at finite lattice spacing and furthermore shows restored supersymmetry as well as the spontaneously broken chiral symmetry in the continuum limit. The price to pay is a single additional fine tuning parameter. It remains an open question whether further possibilities for the lattice derivative like the Neuberger operator provide a discretization which is free from explicit chiral symmetry breaking and perhaps free from the need for fine tuning, provided that only a mild sign problem is encountered at the same time.

Acknowledgments

We would like to thankfully mention the numerous discussions with Björn Wellegehausen. This work has been supported by the DFG Research Training Group “Quantum and Gravitational Fields” GRK 1523 and DFG grant Wi 777/11. The simulations have been carried out at the Omega cluster of the TPI.

A Conventions and Fierz identities

We choose the Majorana representation

$$\gamma_0 = \sigma_3, \quad \gamma_1 = -\sigma_1, \quad \gamma_* = i\gamma_0\gamma_1 = \sigma_2, \quad C = -i\sigma_2, \quad (\text{A.1})$$

and the conjugate spinor is defined as $\bar{\chi} = \chi^T C$. In the main body of the paper we employ the Fierz relation

$$\psi\bar{\chi} = -\frac{1}{2}\bar{\chi}\psi - \frac{1}{2}(\bar{\chi}\gamma^\mu\psi)\gamma_\mu - \frac{1}{2}(\bar{\chi}\gamma_*\psi)\gamma_*. \quad (\text{A.2})$$

Due to the symmetry properties

$$\bar{\chi}\psi = \bar{\psi}\chi, \quad \bar{\chi}\gamma^\mu\psi = -\bar{\psi}\gamma^\mu\chi, \quad \bar{\chi}\gamma_*\psi = -\bar{\psi}\gamma_*\chi \quad (\text{A.3})$$

the two last terms in (A.2) vanish for $\chi = \psi$ such that

$$\psi\bar{\psi} = -\frac{1}{2}\bar{\psi}\psi \mathbb{1}. \quad (\text{A.4})$$

B Invariance of the action under the second supersymmetry

We will prove the invariance of the on-shell action

$$S[\mathbf{n}, \psi] = \int d^2x \left(\partial_\mu \mathbf{n} \cdot \partial^\mu \mathbf{n} + i\bar{\psi}\not{\partial}\psi + \frac{1}{4}(\bar{\psi}\psi)^2 \right) \quad (\text{B.1})$$

under the second supersymmetry transformations (2.12). The variation of the Lagrangian is¹¹

$$\delta\mathcal{L} = 2i\partial_\mu \mathbf{n} \cdot \partial^\mu (\mathbf{n} \times \bar{\varepsilon}\psi) - 2i\bar{\psi}\not{\partial}(\mathbf{n} \times \not{\partial}\mathbf{n}\varepsilon) + 2\bar{\psi}\not{\partial}(\bar{\varepsilon}\psi \times \psi) - (\bar{\psi}\psi) \bar{\psi}(\mathbf{n} \times \not{\partial}\mathbf{n}\varepsilon). \quad (\text{B.2})$$

The term $\propto \psi^5$ vanishes, since ψ is a Grassmannian field with only four independent degrees of freedom. We will see that the first and second term cancel each other as well as the third and fourth one. Starting with the first two terms, they can be written as

$$2i\partial_\mu \mathbf{n}(\mathbf{n} \times \bar{\varepsilon}\partial^\mu \psi) - 2i\bar{\psi}(\mathbf{n} \times \partial^2 \mathbf{n}\varepsilon) - 2i\bar{\psi}\gamma^\mu\gamma^\nu \varepsilon(\partial_\mu \mathbf{n} \times \partial_\nu \mathbf{n}). \quad (\text{B.3})$$

The last term vanishes since $\partial_\mu \mathbf{n} \times \partial_\nu \mathbf{n}$ is parallel to \mathbf{n} and hence perpendicular to ψ . Integrating the second term by parts one sees that the first and second term cancel owing to the cyclicity of the triple product.

¹¹up to a negligible boundary term $\partial_\mu(-\bar{\psi}\gamma^\mu(\bar{\varepsilon}\psi \times \psi^\alpha))$

The cancellation of the third and fourth term in (B.2) is a bit more involved. First, we partially integrate the third term and obtain $-2\partial_\mu \bar{\psi} \gamma^\mu (\bar{\varepsilon} \psi \times \psi)$. Since $\mathbf{n} \cdot \psi^\alpha = 0$ for both spinor components α , we conclude that $\bar{\varepsilon} \bar{\psi} \times \psi$ is parallel to \mathbf{n} such that

$$-2\partial_\mu \bar{\psi} \gamma^\mu (\bar{\varepsilon} \psi \times \psi) = -2(\partial_\mu \bar{\psi} \gamma^\mu \mathbf{n}) \mathbf{n} (\bar{\varepsilon} \psi \times \psi). \quad (\text{B.4})$$

The condition $\bar{\psi} \mathbf{n} = 0$ implies $\partial_\mu \bar{\psi} \mathbf{n} = -\bar{\psi} \partial_\mu \mathbf{n}$. (B.4) can hence be written as $2(\bar{\psi} \not{\partial} \mathbf{n}) \mathbf{n} (\bar{\varepsilon} \psi \times \psi)$. To proceed further, we utilize $\bar{\psi}_1 n_1 = -\bar{\psi}_2 n_2 - \bar{\psi}_3 n_3$ and the Fierz relation $\bar{\psi}_i \gamma^\mu \psi_i = 0$:

$$\begin{aligned} & 2(\bar{\psi}_1 \not{\partial} n_1 + \bar{\psi}_2 \not{\partial} n_2 + \bar{\psi}_3 \not{\partial} n_3) [n_1 \bar{\varepsilon} \psi_2 \cdot \psi_3 - n_1 \bar{\varepsilon} \psi_3 \cdot \psi_2 + \text{cyclic terms}] \\ &= 2\bar{\psi}_2 \gamma^\mu \psi_3 (\partial_\mu n_2 \cdot n_1 - \partial_\mu n_1 \cdot n_2) \bar{\varepsilon} \psi_2 + 2\bar{\psi}_3 \gamma^\mu \psi_2 (\partial_\mu n_1 \cdot n_3 - \partial_\mu n_3 \cdot n_1) \bar{\varepsilon} \psi_3 + \text{cyclic terms}. \end{aligned} \quad (\text{B.5})$$

Finally, we employ the Fierz relation $(\bar{\alpha} \gamma^\mu \beta) \bar{\varepsilon} \alpha = \frac{1}{2} \bar{\alpha} \alpha (\bar{\beta} \gamma^\mu \varepsilon)$, which holds for Majorana spinors, and obtain

$$(\bar{\psi}_2 \psi_2) \bar{\psi}_3 \gamma^\mu \varepsilon (n_1 \partial_\mu n_2 - n_2 \partial_\mu n_1) + (\bar{\psi}_3 \psi_3) \bar{\psi}_2 \gamma^\mu \varepsilon (n_3 \partial_\mu n_1 - n_1 \partial_\mu n_3) + \text{cyclic terms}.$$

Finally, using $(\bar{\alpha} \alpha) \bar{\alpha} = 0$ we obtain for the third term in (B.2) the simple expression

$$(\bar{\psi} \psi) \bar{\psi} (\mathbf{n} \times \not{\partial} \mathbf{n} \varepsilon). \quad (\text{B.6})$$

As a result, the third and fourth term in (B.2) cancel each other. This proves that the action is invariant under the second supersymmetry transformation (2.12).

The invariance of the constraints can be shown easily:

$$\begin{aligned} \delta(\mathbf{n}^2) &= 2i\mathbf{n} \cdot (\mathbf{n} \times \bar{\varepsilon} \psi) = 0 \\ \delta(\mathbf{n} \cdot \psi) &= i(\mathbf{n} \times \bar{\varepsilon} \psi) \cdot \psi - \mathbf{n} \cdot (\mathbf{n} \times \not{\partial} \mathbf{n} \varepsilon) - i\mathbf{n} \cdot (\bar{\varepsilon} \psi \times \psi) = 0. \end{aligned}$$

C Transformation of the discretized measure

The transformation from the constrained fields (\mathbf{n}, ψ) to the unconstrained fields $(\mathbf{u}, \boldsymbol{\lambda})$ has a non-trivial Jacobian. Since the transformation only relates values of the fields on a fixed lattice site it is sufficient to calculate the Jacobian for a given site. Denoting values of the fields on this site by

$$\mathbf{n} = \begin{pmatrix} n_1 \\ \mathbf{n}_\perp \end{pmatrix}, \quad \psi = \begin{pmatrix} \psi_1 \\ \psi_\perp \end{pmatrix}$$

we are lead to consider

$$\begin{aligned} \delta(\mathbf{n}^2 - 1) \delta(\mathbf{n} \cdot \psi^1) \delta(\mathbf{n} \cdot \psi^2) &= \frac{1}{2|n_1|} \left[\delta\left(n_1 - \sqrt{1 - \mathbf{n}_\perp^2}\right) + \delta\left(n_1 + \sqrt{1 - \mathbf{n}_\perp^2}\right) \right] \\ &\quad \cdot \prod_\alpha n_1 \delta\left(\psi_1^\alpha + \frac{\mathbf{n}_\perp \cdot \psi_\perp^\alpha}{n_1}\right). \end{aligned}$$

Consequently, the measure on a given site transforms as

$$d\mathbf{n} d\psi^1 d\psi^2 \delta(\mathbf{n}^2 - 1) \delta(\mathbf{n} \cdot \psi^1) \delta(\mathbf{n} \cdot \psi^2) = \frac{1}{2} J(\mathbf{u}) d\mathbf{u} d\boldsymbol{\lambda}^1 d\boldsymbol{\lambda}^2 \quad (\text{C.1})$$

with Jacobian

$$J(\mathbf{u}) = \sqrt{1 - \mathbf{n}_\perp^2(\mathbf{u})} \left| \text{sdet}\{(\mathbf{n}_\perp, \psi_\perp) \rightarrow (\mathbf{u}, \boldsymbol{\lambda})\} \right|. \quad (\text{C.2})$$

In the super-stereographic projection (2.7) \mathbf{n} does not depend on $\boldsymbol{\lambda}^\alpha$, and ψ^α does not depend on $\boldsymbol{\lambda}^\beta$ for $\beta \neq \alpha$. The superdeterminant is hence given by

$$\text{sdet}\{(\mathbf{n}_\perp, \psi_\perp) \rightarrow (\mathbf{u}, \boldsymbol{\lambda})\} = \frac{\det(\partial \mathbf{n}_\perp / \partial \mathbf{u})}{\det(\partial \psi_\perp^1 / \partial \boldsymbol{\lambda}^1) \cdot \det(\partial \psi_\perp^2 / \partial \boldsymbol{\lambda}^2)}. \quad (\text{C.3})$$

In an $O(N)$ model, all three determinants are equal to

$$(2\rho)^{N-1} \frac{1 - \mathbf{u}^2}{1 + \mathbf{u}^2} \quad \text{with} \quad \rho = \frac{1}{1 + \mathbf{u}^2}.$$

Expressing the square root in (C.2) in terms of the new fields,

$$\sqrt{1 - \mathbf{n}_\perp^2} = \frac{1 - \mathbf{u}^2}{1 + \mathbf{u}^2},$$

we end up with the Jacobian

$$J(\mathbf{u}) = \frac{1}{(2\rho)^{N-1}} \propto (1 + \mathbf{u}^2)^{N-1}. \quad (\text{C.4})$$

The functional integral measure for the supersymmetric $O(3)$ model with unconstrained fields is thus

$$\prod_x d\mathbf{u}_x d\boldsymbol{\lambda}_x^1 d\boldsymbol{\lambda}_x^2 (1 + \mathbf{u}_x^2)^2. \quad (\text{C.5})$$

Note that we proved on the way that the Jacobian for the purely bosonic $O(N)$ model is

$$J_B(\mathbf{u}) \propto \rho^{N-1} = \frac{1}{(1 + \mathbf{u}^2)^{N-1}}. \quad (\text{C.6})$$

D Sign of the fermion determinant

In order to check whether the sign-quenched approximation is applicable in case of the SLAC derivative, simulations on lattice sizes ranging from 5×5 to 11×11 have been performed over a coupling range $g^{-2} \in [0.4, 1.2]$. The results that are based on 10^5 configurations per data point (see Fig. 18, left panel) indicate that the average sign of the Pfaffian is smaller for smaller g^{-2} , which is equivalent to coarser lattices. The problem is that the sign problem worsens for larger lattice volumes at fixed coupling. In these cases the probability based, i.e. sign-quenched, Monte-Carlo sampling will *not* correspond to the relevant configurations in an unquenched ensemble and statistical errors on reweighted measurements will become rather large. Nevertheless, with standard Monte-Carlo techniques simulations are only possible without taking the sign into account, such that a reweighting becomes unavoidable. The discretization based on the SLAC derivative becomes thus unfeasible for larger lattices, which we require in order to study the continuum limit and a possible restoration of supersymmetry there. As a consequence, we have to rely for this purpose on the Wilson derivative only. The average Pfaffian sign for the Wilson derivative is depicted in the right panel of Fig. 18. We see that for small values of the finetuning parameter κ ,

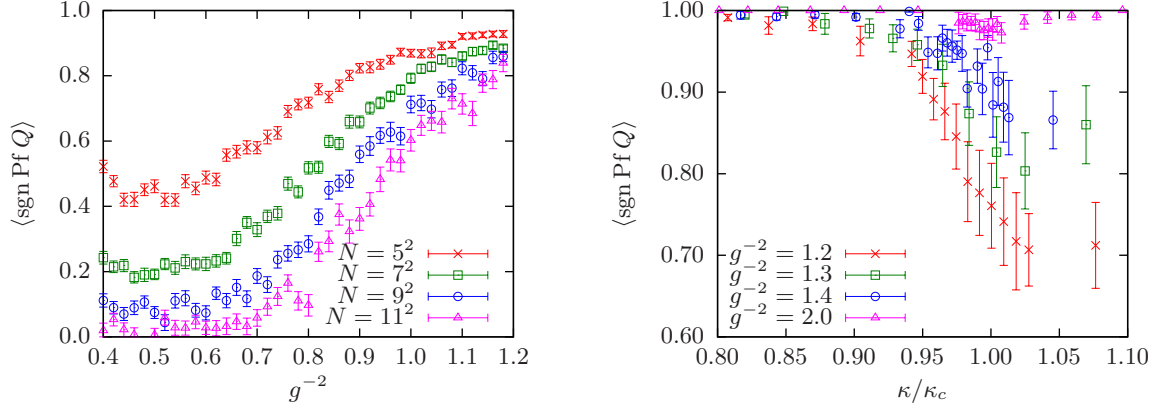


Figure 18. Left Panel: Average sign of the SLAC Pfaffian for different couplings g^{-2} on lattices sizes ranging from 5×5 to 11×11 . Right Panel: Sign of the Wilson Pfaffian on a $N = 16^2$ lattice for different couplings g^{-2} and normalized finetuning parameter κ/κ_c .

which correspond to little finetuning, changes in the Pfaffian sign are suppressed and it is possible to evaluate expectation values directly without the need of reweighting. In the vicinity of $\kappa \approx \kappa_c$ however, this behaviour changes to a mild correction for large coupling $g^{-2} = 2$ up to a significant correction for smaller coupling $g^{-2} = 1.2$. In the finetuned ensemble at $\kappa = \kappa_c$, we regain a sign problem as shown in figure 19. However, even for lattice volume $N = 16^2$ and reasonable box sizes, the average sign for Wilson fermions lies considerably above the SLAC data at lattice volume 11^2 . Also, the Wilson $N = 24^2$ data does not indicate a drastic decrease of the average sign for larger lattices, as seen in the SLAC case. Additionally, applying the Wilson formulation allows for an efficient even-odd preconditioning scheme, which provides a sufficient speed-up in order to account for the larger configuration numbers that are needed for the reweighting procedure.

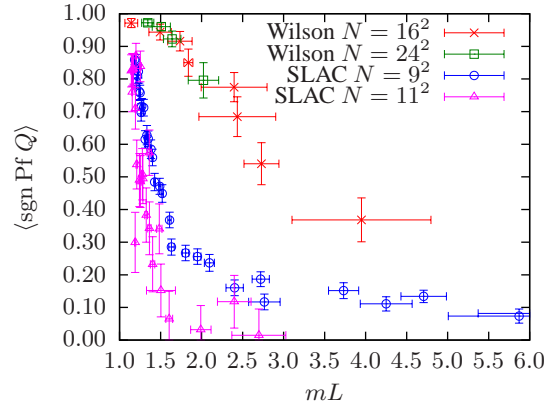


Figure 19. Average Pfaffian sign for different box sizes. Wilson sign data is gathered from the finetuned ensemble at κ_c .

E Algorithmic aspects

We argued in section 3.2 that it is of considerable importance to tune the many technical parameters of advanced algorithms like Rational Hybrid Monte Carlo (RHMC) in the right way in order to obtain an appropriate algorithm that parses configuration space in the correct way. With the sign problem and large condition numbers lurking, a Hybrid Monte Carlo algorithm with exact evaluation of the fermion determinant and the inverse fermion matrix using efficient LAPACK routines was used at small lattice volumes up to 16^2 in order to provide a solid ground for the implementation of more sophisticated pseudofermion algorithms, e.g. RHMC. These algorithms become necessary

at large volumes due to the poor scaling behaviour of the LU decomposition used to solve for the inverse fermion matrix. However, no efficient preconditioning schemes exist for the nonlocal SLAC derivative. Therefore we concentrated our efforts on the Wilson derivative which allows for even-odd preconditioning and, moreover, shows less severe sign problems at finite volume. In Table 2

	original	reduced	even-odd
condition number	$1.6(6) \cdot 10^{19}$	$1.3(6) \cdot 10^8$	$1.4(7) \cdot 10^3$
cg solver steps	454(10)	152(1)	48(1)

Table 2. Average condition numbers and CG solver steps for three different choices of fermion matrix formulation.

average condition numbers κ obtained from the exact matrix norm $\kappa = \|Q\| \cdot \|Q^{-1}\|$ are shown as well as typical iteration numbers of a conjugate gradient solver for three different choices of the fermion matrix: 1. the original fermion matrix, 2. the reduced fermion matrix where a factor ρ , whose determinant can be evaluated analytically, is separated on both sides,

$$Q'^{\alpha\beta}_{xy,ij} = 4(\delta_{ik} - 2u_{x,i}u_{x,k}\rho_x)M_{xy}^{\alpha\beta}(\delta_{kj} - 2u_{y,k}u_{y,j}\rho_y) + 16\rho_x u_{x,i}M_{xy}^{\alpha\beta}u_{y,j}\rho_y + 4\beta\sigma_x\delta_{xy}\delta_{ij}\delta^{\alpha\beta}, \quad (\text{E.1})$$

and 3. the preconditioned reduced fermion matrix using the well-known even-odd preconditioning scheme [33]. The critical step of the iterative cg solver is the application of the inverse of $Q^T Q$, which is used in the pseudofermion algorithm, to some random (pseudofermion) vector, $Y = (Q^T Q)^{-1}X$. We see a significant improvement in the number of solver steps and in the condition numbers for the reduced fermion matrix. This can directly be verified by looking at the eigenvalue spectrum depicted in figure 20. Both matrices, the original and the reduced one, are real and

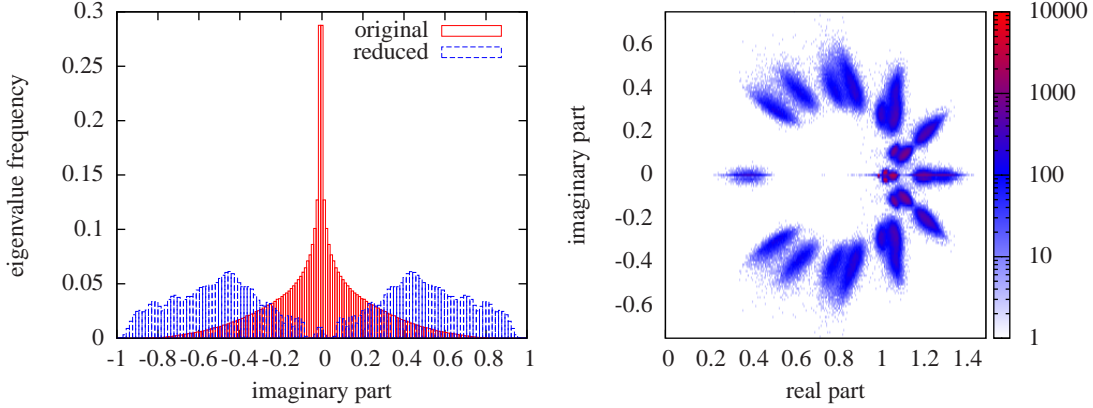


Figure 20. Eigenvalue frequency of the original and reduced fermion matrix (left panel, normalized such that both the largest eigenvalue and the integrated surface equal one) and for the even-odd preconditioned matrix (right panel, no normalization, logarithmic scale) from a sample of 2000 configurations on a 12^2 lattice.

antisymmetric, so that all eigenvalues are purely imaginary and come in complex conjugate pairs. Whereas the original fermion matrix exhibits a large number of eigenvalues very close to zero¹²,

¹²This is expected according to the Banks-Casher-relation.

this is not the case for the reduced one and the condition numbers hence decrease drastically. A further improvement is achieved by even-odd preconditioning. The preconditioned matrix is no longer antisymmetric and we see that the majority of eigenvalues lie close to 1. This is what we expected, since the goal of the incomplete LU preconditioning [34, 35], which can be regarded as a generalization of the even-odd scheme, is to rewrite the fermion matrix in the form $1 - L - U$, where 1 is the identity matrix and L (U) is a lower (upper) triangular matrix.

References

- [1] N. Arkani-Hamed, D. P. Finkbeiner, T. R. Slatyer, and N. Weiner, *A Theory of Dark Matter*, *Phys. Rev. D* **79** (2009) 015014, [[arXiv:0810.0713](#)].
- [2] J. E. Kim and G. Carosi, *Axions and the strong CP problem*, *Rev. Mod. Phys.* **82** (Mar, 2010) 557–601, [[arXiv:0807.3125](#)].
- [3] V. A. Novikov, M. A. Shifman, A. I. Vainshtein, and V. I. Zakharov, *Two-Dimensional Sigma Models: Modeling Nonperturbative Effects of Quantum Chromodynamics*, *Phys. Rept.* **116** (1984) 103.
- [4] E. Witten, *A Supersymmetric Form of the Nonlinear Sigma Model in Two- Dimensions*, *Phys. Rev. D* **16** (1977) 2991.
- [5] P. Di Vecchia and S. Ferrara, *Classical Solutions in Two-Dimensional Supersymmetric Field Theories*, *Nucl. Phys. B* **130** (1977) 93.
- [6] R. Shankar and E. Witten, *S matrix of the supersymmetric nonlinear σ model*, *Phys. Rev. D* **17** (Apr, 1978) 2134–2143.
- [7] O. Alvarez, *Dynamical symmetry breakdown in the supersymmetric nonlinear σ model*, *Phys. Rev. D* **17** (Feb, 1978) 1123–1130.
- [8] J. M. Evans and T. J. Hollowood, *The Exact mass gap of the supersymmetric $O(N)$ sigma model*, *Phys. Lett. B* **343** (1995) 189–197, [[hep-th/9409141](#)].
- [9] B. Zumino, *Supersymmetry and Kähler Manifolds*, *Phys. Lett. B* **87** (1979) 203.
- [10] P. H. Dondi and H. Nicolai, *Lattice supersymmetry*, *Nuovo Cim. A* **41** (1977) 1.
- [11] I. Montvay, *Tuning to $N=2$ supersymmetry in the $SU(2)$ adjoint Higgs-Yukawa model*, *Nucl. Phys. B* **445** (1995) 399–428, [[hep-lat/9503009](#)].
- [12] S. Catterall, D. B. Kaplan, and M. Unsal, *Exact lattice supersymmetry*, *Phys. Rept.* **484** (2009) 71–130, [[arXiv:0903.4881](#)].
- [13] S. Catterall and S. Ghadab, *Lattice sigma models with exact supersymmetry*, *JHEP* **05** (2004) 044, [[hep-lat/0311042](#)].
- [14] S. Catterall and S. Ghadab, *Twisted supersymmetric sigma model on the lattice*, *JHEP* **10** (2006) 063, [[hep-lat/0607010](#)].
- [15] T. Kästner, G. Bergner, S. Uhlmann, A. Wipf, and C. Wozar, *Two-Dimensional Wess-Zumino Models at Intermediate Couplings*, *Phys. Rev. D* **78** (2008) 095001, [[arXiv:0807.1905](#)].
- [16] A. Kirchberg, J. D. Lange, and A. Wipf, *From the Dirac operator to Wess-Zumino models on spatial lattices*, *Ann. Phys.* **316** (2005) 357–392, [[hep-th/0407207](#)].
- [17] J. Hubbard, *Calculation of partition functions*, *Phys. Rev. Lett.* **3** (1959) 77–80.

- [18] S. D. Drell, M. Weinstein, and S. Yankielowicz, *Variational approach to strong coupling field theory. I. ϕ^4 theory*, *Phys. Rev.* **D14** (1976) 487.
- [19] G. Bergner, T. Kästner, S. Uhlmann, and A. Wipf, *Low-dimensional supersymmetric lattice models*, *Annals Phys.* **323** (2008) 946–988, [[arXiv:0705.2212](#)].
- [20] C. Wozar and A. Wipf, *Supersymmetry Breaking in Low Dimensional Models*, *Annals Phys.* **327** (2012) 774–807, [[arXiv:1107.3324](#)].
- [21] M. Lüscher, P. Weisz, and U. Wolff, *A Numerical method to compute the running coupling in asymptotically free theories*, *Nucl. Phys.* **B359** (1991) 221–243.
- [22] J. Balog, F. Niedermayer, and P. Weisz, *The puzzle of apparent linear lattice artifacts in the 2d non-linear sigma-model and Symanzik’s solution*, *Nucl. Phys.* **B824** (2010) 563–615, [[arXiv:0905.1730](#)].
- [23] U. Wolff, *Simulating the All-Order Strong Coupling Expansion III: $O(N)$ sigma/loop models*, *Nucl. Phys.* **B824** (2010) 254–272, [[arXiv:0908.0284](#)].
- [24] J. Balog and A. Hegedus, *TBA equations for excited states in the $O(3)$ and $O(4)$ nonlinear sigma-model*, *J. Phys.* **A37** (2004) 1881–1901, [[hep-th/0309009](#)].
- [25] M. Hasenbusch, P. Hasenfratz, F. Niedermayer, B. Seefeld, and U. Wolff, *Nonstandard cutoff effects in the nonlinear sigma model*, *Nucl. Phys. Proc. Suppl.* **106** (2002) 911–913, [[hep-lat/0110202](#)].
- [26] G. Bergner, *Complete supersymmetry on the lattice and a No-Go theorem: A simulation with intact supersymmetries on the lattice*, *JHEP* **01** (2010) 024, [[arXiv:0909.4791](#)].
- [27] N. D. Mermin and H. Wagner, *Absence of ferromagnetism or antiferromagnetism in one- dimensional or two-dimensional isotropic Heisenberg models*, *Phys. Rev. Lett.* **17** (1966) 1133–1136.
- [28] F. Sugino, *A lattice formulation of super Yang-Mills theories with exact supersymmetry*, *JHEP* **01** (2004) 015, [[hep-lat/0311021](#)].
- [29] J. M. Evans and T. J. Hollowood, *The Exact mass gap of the supersymmetric CP^{n-1} sigma model*, *Phys. Lett.* **B343** (1995) 198–206, [[hep-th/9409142](#)].
- [30] E. Witten, *Constraints on Supersymmetry Breaking*, *Nucl. Phys.* **B202** (1982) 253.
- [31] A. Donini, M. Guagnelli, P. Hernandez, and A. Vladikas, *Towards $N=1$ Super-Yang-Mills on the lattice*, *Nucl.Phys.* **B523** (1998) 529–552, [[hep-lat/9710065](#)].
- [32] M. A. Clark and A. D. Kennedy, *Accelerating dynamical fermion computations using the rational hybrid Monte Carlo (RHMC) algorithm with multiple pseudofermion fields*, *Phys. Rev. Lett.* **98** (2007) 051601, [[hep-lat/0608015](#)].
- [33] T. A. DeGrand and P. Rossi, *Conditioning techniques for dynamical fermions*, *Comput.Phys.Commun.* **60** (1990) 211–214.
- [34] Y. Oyanagi, *An incomplete LDU decomposition of lattice fermions and its application to conjugate residual methods*, *Comput.Phys.Commun.* **42** (1986), no. 3 333 – 343.
- [35] M. J. Peardon, *Accelerating the hybrid Monte Carlo algorithm with ILU preconditioning*, [[hep-lat/0011080](#)].